

Received: 5 September 2014 – Accepted: 25 September 2014 – Published: 15 October 2014

Correspondence to: L. Istomina (lora@iup.physik.uni-bremen.com)

Published by Copernicus Publications on behalf of the European Geosciences Union.

Discussion Paper | Discussion Paper | Discussion Paper | Discussion Paper

TCD

8, 5227–5292, 2014

**The melt pond
fraction and spectral
sea ice albedo
retrieval from MERIS
data**

L. Istomina et al.

Title Page

Abstract

Introduction

Conclusions

References

Tables

Figures



Back

Close

Full Screen / Esc

Printer-friendly Version

Interactive Discussion

5228



Abstract

The presence of melt ponds on the Arctic sea ice strongly affects the energy balance of the Arctic Ocean in summer. It affects albedo as well as transmittance through the sea ice, which has consequences on the heat balance and mass balance of sea ice. An algorithm to retrieve melt pond fraction and sea ice albedo (Zege et al., 2014) from the MEdium Resolution Imaging Spectrometer (MERIS) data is validated against aerial, ship borne and in situ campaign data. The result show the best correlation for landfast and multiyear ice of high ice concentrations (albedo: $R = 0.92$, RMS = 0.068, melt pond fraction: $R = 0.6$, RMS = 0.065). The correlation for lower ice concentrations, subpixel ice floes, blue ice and wet ice is lower due to complicated surface conditions and ice drift. Combining all aerial observations gives a mean albedo RMS equal to 0.089 and a mean melt pond fraction RMS equal to 0.22. The in situ melt pond fraction correlation is $R = 0.72$ with an RMS = 0.14. Ship cruise data might be affected by documentation of varying accuracy within the ASPeCT protocol, which is the reason for discrepancy between the satellite value and observed value: mean $R = 0.21$, mean RMS = 0.16. An additional dynamic spatial cloud filter for MERIS over snow and ice has been developed to assist with the validation on swath data. The case studies and trend analysis for the whole MERIS period (2002–2011) show pronounced and reasonable spatial features of melt pond fractions and sea ice albedo. The most prominent feature is the melt onset shifting towards spring (starting already in weeks 3 and 4 of June) within the multiyear ice area, north to the Queen Elizabeth Islands and North Greenland.

1 Introduction

Melt ponds on the Arctic sea ice affect the albedo, mass balance and heat balance of the ice (e.g. Perovich et al., 2009) by translating the increase of air temperature into drastic and rapid surface type changes. They introduce a positive feedback within the sea ice albedo feedback loop (Curry et al., 1995) thus facilitating further ice melt.

The melt pond fraction and spectral sea ice albedo retrieval from MERIS data

L. Istomina et al.

Title Page

Abstract

Introduction

Conclusions

References

Tables

Figures

◀

▶

◀

▶

Back

Close

Full Screen / Esc

Printer-friendly Version

Interactive Discussion



The melt pond fraction and spectral sea ice albedo retrieval from MERIS data

L. Istomina et al.

Title Page

Abstract

Introduction

Conclusions

References

Tables

Figures

◀

▶

◀

▶

Back

Close

Full Screen / Esc

Printer-friendly Version

Interactive Discussion

In the context of changing Arctic climate (Shindell and Faluvegi, 2009), knowledge of melt pond fraction (MPF), its spatial distribution and the length of the melting season is required to reflect and predict the role of the sea ice cover in the radiative balance of the region. Schröder et al. (2014) show the potential of predicting the minimum sea ice extent in autumn by spring MPF. In addition to applications in climate studies, e.g. global circulation modeling, knowledge of MPF can be helpful for navigation purposes.

The present work is dedicated to validation and application of a MPF and sea ice albedo retrieval algorithm, the Melt Pond Detector (MPD), described by Zege et al. (2014). The algorithm differs from existing remote sensing algorithms (e.g. Rösel et al., 2012; Tschudi et al., 2008), by (1) utilizing a physical model of sea ice and melt ponds with no a priori surface parameters and (2) providing daily averaged MPF instead of weekly averaged MPF, which is beneficial in case of rapid melt evolution. Field observations (Fig. 1) show faster melt evolution on first year ice (FYI) as compared to multiyear ice (MYI). Due to the fact that MPF depends not only on air temperature and available melt water volume but also on the ice topography (Eicken et al., 2004; Polashenski et al., 2012), melt evolution is different for FYI and MYI. Melt onset proceeds rapidly to the MPF maximum on FYI with rapid pond drainage and moderate MPFs afterwards. On multiyear ice, the evolution of melt up to the melt maximum takes longer. The peak MPF value is lower and the MPF decrease is slower than that on FYI (Fig. 1). A detailed description of melt stages and melt water distribution mechanisms can be found in Polashenski et al. (2012). These details of melt evolution create spatial variability of MPF and sea ice albedo, and air mass transport and changing air temperature is main driver of the temporal variability of the MPF. This introduces complications in the MPF modeling and creates the need for a satellite retrieval of MPF and sea ice albedo of possibly high temporal and spatial resolution.

The manuscript is structured as follows: in Sect. 2 the MPD algorithm, its input and output data are described. Section 3 is dedicated to validation of the albedo (Sect. 3.1) and MPF (Sect. 3.2) products. The additional cloud screening developed for the purpose of quality validation is presented in Sect. 3.2.2. The case studies (Sect. 4) consist

of comparison of the MPF and albedo data to the reanalysis air temperature (Sect. 4.2). Global applications of the MPD algorithms over the whole MERIS dataset (2002–2011) are given in Sect. 5. There the weekly averages for 2007 and 2011 are analyzed (Sect. 5.1), trends of MPF (Sect. 5.2) and sea ice albedo (Sect. 5.3). The conclusions are given in Sect. 6.

2 Data used

The data used for the present study are the pond fraction and broadband sea ice albedo swath data products retrieved from MERIS swath Level 1b data over the ice covered Arctic Ocean using the MPD retrieval.

The MPD is a new algorithm for retrieving characteristics (albedo and melt ponds fraction) of summer melting ice in the Arctic from data of satellite spectral instruments. In contrast to other algorithms (Rösel et al., 2012; Tschudi et al., 2008) MPD does not use a priori values of the spectral albedo of constituents of the melting ice (melt ponds, drained surface, etc.) but it is based on the theory of their optical properties.

The retrieval algorithm is based on the observations of optical properties of constituents of sea-ice (Perovich, 1996). A pixel is considered as consisting of two constituents: white ice and melt ponds. The reflection properties of surface is described by the spectral bi-directional reflectance distribution function (BRDF) $R(\theta, \theta_0, \varphi, \lambda)$, where θ and θ_0 are the zenith angles of the observation and illumination directions, respectively, and φ is the azimuth angle between them, λ is the wavelength.

The white ice is considered as an optically thick weakly absorbing layer. The BRDF of this sub-pixel $R_{ice}(\theta, \theta_0, \varphi, \lambda)$ is determined by its optical depth τ_{wi} , the mean effective grain size a_{eff} , and the absorption coefficient α_{yp} of yellow pigments, which could arise due to sediments from the seawater. The spectral dependencies of optical characteristics of a layer are determined by the spectrum of the complex refractive index of ice by Warren and Brandt (2008) and spectral absorption of yellow pigments by Bricaud et al. (1981). The used analytical approximation for $R_{ice}(\theta, \theta_0, \varphi, \lambda)$ has been

The melt pond fraction and spectral sea ice albedo retrieval from MERIS data

L. Istomina et al.

Title Page

Abstract

Introduction

Conclusions

References

Tables

Figures

◀

▶

◀

▶

Back

Close

Full Screen / Esc

Printer-friendly Version

Interactive Discussion

developed on the base of the asymptotic solution of the radiative transfer theory (Zege et al., 1991).

The BRDF of a melt pond $R_{\text{pond}}(\theta, \theta_0, \varphi, \lambda)$ is determined by the melt water optical depth τ_p and by the spectral albedo of its bottom. The pond bottom is an ice layer, which in turn is characterized by the transport scattering coefficient σ_{ice} and the optical depth τ_{ice} . Thus, the BRDF of the melt pond is calculated as reflection of the water layer with a semi-translucent bottom.

It is supposed that the pixel surface consists of white ice (highly reflective) and melt ponds with area fraction S . The BRDF of the whole pixel is a linear combination:

$$R(\theta, \theta_0, \varphi, \lambda) = (1 - S)R_{\text{ice}}(\theta, \theta_0, \varphi, \lambda) + SR_{\text{pond}}(\theta, \theta_0, \varphi, \lambda). \quad (1)$$

The body of the retrieval algorithm comprises of the following steps.

1. The input to the algorithm is the MERIS level 1B data, including the radiance coefficients R_i at channels $i = 1, 2, 3, 4, 8, 10, 12, 13, 14$, and the solar and observation angles (zenith and azimuth). Also the relevant information on atmosphere and surface state can be entered from an input file.
2. The data is sent to the three independent blocks:
 - a. The atmospheric correction preprocessing block. The atmosphere reflectance r_i and transmittance t_i are calculated for the used set of wavelengths (i is the channel number). Atmospheric correction is performed with regard to the surface BRDF.
 - b. Separation of the sea-ice pixels. In this procedure the ice pixels are separated from the cloud, land and open water pixels, using the brightness criterion on the channels R_2, R_3 , and R_4 , spectral neutrality criterion on the ratio of the channels R_1 and R_2 , MERIS differential snow index (Schlundt et al., 2011) and the threshold on the ratio of the MERIS oxygen-A band (R_{11} and R_{10}). The first two criteria separate white surfaces, which can be snow, ice,

The melt pond fraction and spectral sea ice albedo retrieval from MERIS data

L. Istomina et al.

Title Page

Abstract

Introduction

Conclusions

References

Tables

Figures

◀

▶

◀

▶

Back

Close

Full Screen / Esc

Printer-friendly Version

Interactive Discussion



typical situations, including “standard” white ice, bright ice (snow covered), dark and light blue melt ponds. The numerical experiment showed that the melt pond fraction can be retrieved with high accuracy (error less than 1 %) for the most common case of “standard” white ice and light blue (young) melt pond. The retrieval error increases with deviation from the “standard” case, e.g. the retrieved pond fraction can be underestimated more than twice for the case of bright (snow covered) ice and dark (mature) melt pond. However, this situation is rare, because a mature pond is formed in the process of the developed melt, when snowfalls are not very often. At the same time the MPD algorithm provides accurate retrievals of the spectral albedo in all considered cases, even in the situations when the error of the pond fraction retrieval is maximal. The spectral albedo is retrieved much better with the MPD algorithm than within the conventional algorithms using the Lambert approximation for surface reflection, which underestimates the albedo at about 0.05 all over the spectral range, whereas the error of the MPD retrieval in the worst case (“bright ice – dark pond”) is 0.01 and lower in all other considered cases.

3 Validation

The datasets used for the validation of the MPD algorithm are shown in Table 1.

These validation datasets contain a wide range of pond fractions and were obtained over landfast ice, FYI and MYI of various ice concentrations. Therefore the performance of the satellite retrieval can be thoroughly tested for a variety of conditions and conclusions on the more or less suitable conditions for the application of the MPD retrieval can be drawn. Such conclusions are especially important as the MPD retrieval was designed for a limited set of ice and pond parameters, namely for the conditions of the melt evolution with open melt ponds surrounded by dry white ice in the high Arctic within the pack ice. A sensitivity study based on modeled input data shows the algorithm’s better performance for bright melt ponds as opposed to dark melt ponds (Zege et al., 2014). Therefore, it is expected that the MPD algorithm shows the best performance over MYI

The melt pond fraction and spectral sea ice albedo retrieval from MERIS data

L. Istomina et al.

Title Page

Abstract

Introduction

Conclusions

References

Tables

Figures

◀

▶

◀

▶

Back

Close

Full Screen / Esc

Printer-friendly Version

Interactive Discussion



The melt pond fraction and spectral sea ice albedo retrieval from MERIS data

L. Istomina et al.

Title Page

Abstract

Introduction

Conclusions

References

Tables

Figures

◀

▶

◀

▶

Back

Close

Full Screen / Esc

Printer-friendly Version

Interactive Discussion



measurements is very limited, and for those available, the question of how representative the chosen transect is for the whole area is anyway present. In this study, we use a transect data taken in Canadian Arctic in June and July 2006 as part of the joint Finnish Institute of Marine Research and University of Calgary Cryosphere Climate Research Group polar ice POL-ICE research project (Geldsetzer et al., 2006), where the uniform pond distribution was confirmed using helicopter images (not shown here).

During POL-ICE 2006 the spatio-temporal evolution of surface features and their spectral reflectance properties were monitored by collecting a series of transect measurements on landfast FYI (FI) also in the vicinity of Resolute Bay, Nunavut between 26 June 2006 and 11 July 2006. For each transect, a 200 m transect line was established perpendicular to the predominant major-axis pond direction to maximize the frequency of changes between ponds and snow/bare ice patches. For the relatively uniformly distributed network of ponds and snow/bare ice patches characteristics of smooth FYI, this orientation yields a representative areal fraction of cover types (Grenfell and Perovich, 2004). A total of 12 transects were collected with surface cover types classified as: melt pond, snow/bare ice, or mixed at 0.5 m intervals. The mixed cover type was introduced to classify the slushy mixture of saturated ice that could be neither classed as discrete pond or snow/bare ice. The data is shown in Table 2.

For 8 of POL-ICE 2006 transects and when lighting conditions were suitable, cosine-corrected downwelling and upwelling radiance (0.35 m height) measurements were made at 2 m intervals using a TriOS RAMSES spectrometer (320–950 nm). Spectral data were processed using the calibration files and software bundled with the RAMSES spectrometer, with radiation measurements integrated across the bandwidth of the instrument to create integrated albedo measurements from each sample. Each albedo measurement was matched to a surface class, and average broadband albedo statistics by class and for each transect were derived. For these locations, the MPD retrieval has been performed and the broadband albedo average within 5 km around the location has been produced. Satellite overflights closest in time to the field measurements were taken. The result is shown in Table 3. The gaps in the retrieved data

are due to cloud cover. The discrepancies between the field and satellite albedo can be explained by difference in the spatial resolution of the two datasets and varying melt pond distribution within the studied area.

3.1.2 Aerial validation

5 The validation has been performed for selected cloud free satellite swaths at the reduced resolution of the retrieval (MERIS data, reduced resolution, 1.2km × 1.2km).

The aircraft campaign MELTEX (“Impact of melt ponds on energy and momentum fluxes between atmosphere and sea ice”) was conducted by the Alfred Wegener Institute for Polar and Marine Research (AWI) in May and June 2008 over the southern Beaufort Sea (Birnbaum et al., 2009).

10 The campaign aimed at improving the quantitative understanding of the impact of melt ponds on radiation, heat, and momentum fluxes over Arctic sea ice. For determining broadband surface albedo, the BASLER BT-67 type aircraft POLAR 5 was equipped with two Eppley pyranometers of type PSP measuring the broadband hemispheric down- and upwelling shortwave radiation. The radiation sensors were mounted on the aircraft in a fixed position. For clear-sky conditions, data of the upward facing pyranometer, which receives direct solar radiation, were corrected for the misalignment of the instrument (based on a method described by Bannehr and Schwiesow, 1993) and the roll and pitch angles of the aircraft to derive downwelling hemispheric radiation flux densities for horizontal exposition of the sensor (see Lampert et al., 2012).

15 Weather conditions in May 2008 were characterized by warming events interrupted by cold-air advection from the inner parts of the Arctic towards the coast of the southern Beaufort Sea. A warming event on 23 May and 24 May 2008, caused the onset of melt pond formation on ice in a large band along the coast from the Amundsen Gulf to Alaska. On 26 May 2008, numerous melt ponds in a very early stage of development were overflowed. However, from 27 May to 1 June 2008, a new period with prevailing cold-air flow caused a refreezing of most melt ponds, which were still very shallow at that time. During the last week of the measurements, a tongue of very warm air was

The melt pond fraction and spectral sea ice albedo retrieval from MERIS data

L. Istomina et al.

Title Page

Abstract

Introduction

Conclusions

References

Tables

Figures

◀

▶

◀

▶

Back

Close

Full Screen / Esc

Printer-friendly Version

Interactive Discussion



shifted from Alaska to the Beaufort Sea. It reached its largest extension over the ocean on 4 and 5 June 2008, which again strongly forced the development of melt ponds.

The available validation data consist of 5 flight tracks for 5 days 26 May 2008, 3, 4, 6 and 7 June 2008. Only the cloud free data is selected. The measurements were performed at different altitudes, as low as 50 m and reaching 400 m, with correspondingly different numbers of measurement points for each satellite pixel. The collocation of such an uneven dataset with the satellite data has been performed by calculating an orthodromic distance of every pixel within a satellite swath to a given aerial measurement point, and collecting those aerial points lying at the minimum distance to the centre of a given satellite pixel. This ensures that aerial measurements performed at any height are collocated to the corresponding satellite pixel correctly. The number of data points per flight is in the order of tens to hundreds of thousands with up to 500 points per satellite pixel.

The validation effort has been done on swath satellite data. The quality of retrieval conditions for the MPD algorithm differ for each overflight depending on weather conditions, ice concentration and ice type. In addition, time difference between the satellite overflight and aerial measurements affect the comparison (Table 4) due to ice drift.

An example of such different conditions is shown in Fig. 3, where the flight tracks over FI and over separate ice floes are shown.

The time difference between the aerial measurement and satellite overflight varies for the presented cases, which adds to the validation data uncertainty for cases with lower ice concentrations due to drifting separate floes. Where possible in case of drift, the time difference was limited to 1.5 h around the satellite overflight. Figure 4 shows the altitude and the correlation of the measured and retrieved broadband albedo for the only flight over FI on 6 June 2008. The rest of the flights were flown over separate floes. They are shown in Figs. 5–7. As no screening of albedo data was possible, it was decided to limit the time difference to 1.5 h around the satellite overflight for the asymmetrically distributed flights. Some points of low measured albedo but high retrieved albedo feature time difference up to 2 h and are most probably connected to the drift

The melt pond fraction and spectral sea ice albedo retrieval from MERIS data

L. Istomina et al.

Title Page

Abstract

Introduction

Conclusions

References

Tables

Figures



Back

Close

Full Screen / Esc

Printer-friendly Version

Interactive Discussion



of separate ice floes. These are flights on 4 June 2008, 26 May 2008, 3 June 2008 and 7 June 2008 (Figs. 5–7). Due to ice drift, the aerial measurements are displaced relative to the satellite snapshot which causes different areas to be compared to each other. The resolution differences of the two sensors may increase this difference even more. Therefore, slight over or underestimation due to the ice concentration difference of aerial and satellite measurements is visible. As the numerical experiment shows that accuracy of the albedo retrieval in all cases is high (Zege et al., 2014), and the case of no drift shows high correlation of retrieved and measured albedo (FI case shown in Fig. 4), we conclude that the discrepancy is due to the specifics of data used for validation and not a weak point of the MPD retrieval.

3.2 Validation of the melt pond product

3.2.1 Aerial validation

For the validation of the melt pond product, the aerial photos from the same airborne campaign MELTEX 2008 have been used. While the flight tracks are the same, the criteria for data selection are different for albedo and melt pond measurements. This is why the validation data for melt pond and albedo data not to overlap entirely for the same flight. The number of points per flight is in the order of hundreds with about 5 images per satellite pixel (example photograph is shown in Fig. 8). Additionally, one more flight over MYI near the coast of North Greenland performed during the aerial campaign NOGRAM-2 2011 has been used.

For the evaluation of the aerial photographs a supervised classification method (maximum likelihood) was applied.

For every pixel x , the probability D belonging to every class c is calculated. The pixels get assigned to the class with the highest probability (Jensen, 2008). For this kind of classification, the training data statistics has to be normally distributed. The maximum likelihood is as follows (Gonzalez and Woods, 2002):

The melt pond fraction and spectral sea ice albedo retrieval from MERIS data

L. Istomina et al.

Title Page

Abstract

Introduction

Conclusions

References

Tables

Figures

◀

▶

◀

▶

Back

Close

Full Screen / Esc

Printer-friendly Version

Interactive Discussion



The melt pond fraction and spectral sea ice albedo retrieval from MERIS data

L. Istomina et al.

Title Page

Abstract

Introduction

Conclusions

References

Tables

Figures

◀

▶

◀

▶

Back

Close

Full Screen / Esc

Printer-friendly Version

Interactive Discussion

$$D = \ln(a_c) - [0.5 \ln(|\mathbf{Cov}_c|)] - [0.5(\mathbf{X} - \mathbf{M}_c)^T (\mathbf{Cov}_c^{-1})(\mathbf{X} - \mathbf{M}_c)] \quad (2)$$

where D is the quantities weighted distance (likelihood), c is a particular class, \mathbf{X} is the measurement vector of the candidate pixel, \mathbf{M}_c is the mean vector of the sample of class c , a_c is the probability that any candidate pixel is a member of class c (was always set to 1 in our calculations), \mathbf{Cov}_c is the covariance matrix of the pixels in the sample of class c , T is the transposition function.

More than 10 000 aerial photographs were recorded during the MELTEX campaign on the different flight tracks. As the quality of the data was not uniform, only images which meet the following requirements were chosen: images taken during horizontal flight tracks (to minimize the geometric distortions) and clear sky flight tracks (to prevent a wrong classification because of fog, clouds and shadows of the clouds). The camera was operated with a non-constant exposure, so that the sea ice in images with a large fraction of open water was overexposed and useless for further evaluation. To simplify the automated classification, images of each day were separated into different flight tracks with similar exposure, ice conditions and same flight level. Nevertheless almost 3000 images were classified and evaluated for the MELTEX campaign. Two suitable flight tracks of the NOGRAM-2 campaign that contain about 1000 images were chosen to complement the quantification of the melt stages. Depending on the flight level, each image covered an area between 0.2 and 3 km².

Overall the validation data used features four types of sea ice: thin and thick FYI as well as fast ice (FI) for the MELTEX images, and MYI for NOGRAM-2. Most of the investigation area of the MELTEX campaign was covered by thin FYI or FI. Only on 7 June 2008, the most northerly part of the flight track contained a notable amount of thick FYI. This part showed a different behavior during the melting process and contained different surface classes than the thin FYI or FI.

Most flight tracks of the campaign were subdivided in several subflight tracks. For every subflight track a representative image was chosen, which contained all classes. Mostly, there were no representative images with all classes for a given subflight track.

Therefore, two or more images were merged for the determination of the training data. The threshold for the maximum likelihood method was set to 0.95. This means that the probability of belonging to a defined class must be 0.95 or higher. Otherwise the pixels were not classified. Within the presented study, the amount of unclassified pixels per image is uniform and is about 1–2 %.

The sea ice conditions varied greatly for each of the studied flights, with the cases range from land fast ice of 100% ice concentration, separate drifting ice floes to thrashed ice with subpixel ice floes (example in Fig. 9). The cases with no separate ice floes and no ice drift are shown in Fig. 10 (FI) and Fig. 11 (left panel, MYI) with quite good correspondence of the retrieved and measured pond fractions. Right panel in Fig. 11, on the other hand, shows higher retrieved MPF than measured from the aircraft. The reason for this discrepancy is twofold: relatively large time difference and the challenging surface conditions. The surface state at the time was as follows: the reported cold air intrusion in the area on 1 June 2008 prevented the forming melt ponds from evolving further (an overview on surface conditions in the area can be found in Scharien et al., 2012), and the large floes were covered with frozen ponds at the beginning of their evolution. Frozen shallow ponds at the beginning of their evolution were classified as sea ice from the aerial images, but retrieved as melt ponds from the satellite. For the applications connected to the radiation budget studies (e.g. GCM), a generalization where darker types of sea ice and melt ponds are put into one class is appropriate due to similar radiative characteristics of the two.

Figure 12 shows the flight on 7 June 2008, which features larger ice floes than the flights shown in Fig. 13. The MPF output of the MPD algorithm is not affected by the subpixel fraction of open water because the almost constant spectrum of open water only affects the amplitude and not the spectral shape of the mixture of surfaces (sea ice, ponds and open water) within the pixel; however, the spectral signature of melt ponds is harder to resolve in case of lower ice concentrations. Subpixel ice floes, thrashed ice with inclusions of blue ice are not appropriate conditions for the MPD algorithm application, hence the overestimated pond fraction for both flights in Fig. 13.

The melt pond fraction and spectral sea ice albedo retrieval from MERIS data

L. Istomina et al.

Title Page

Abstract

Introduction

Conclusions

References

Tables

Figures

◀

▶

◀

▶

Back

Close

Full Screen / Esc

Printer-friendly Version

Interactive Discussion



3.2.2 Cloud screening for in situ and ship cruise validation

As the aerial validation has been performed on cloud free data, the problem of cloud clearing did not arise. For in situ and ship cruise data, cloud contamination may increase the uncertainty of the satellite retrieved values and in these cases this problem has to be addressed additionally. With the gridded product, the unscreened cloud edges and partly screened out clouds are cut out with the criterion for minimum valid data pixels allowed into one grid cell. For the swath data, such criterion is not applied and the existing cloud filtering proved to be not sufficient for a quality validation. Therefore, an additional spatial dynamic filter was introduced for ship cruise and in situ data. An example is shown in Fig. 14.

The dynamic spatial filter consists of dividing the swath into boxes of 10×10 pixels with all the surface and cloud screening criteria applied except the oxygen A filter (Eq. 5 in Zege et al., 2014); due to MERIS bands specifics, all these filters are imperfect and are subject to misclassifying certain types of clouds (e.g. thin clouds and ice clouds) as ice and snow. Then, within a given box, the oxygen A filter is applied. If this additional oxygen A filter screened out some additional pixels, then the box is potentially cloudy and the imperfect cloud filters surely left some unscreened clouds. Such a box is discarded completely. If the additional oxygen A filter (which is more sensitive to high and thick low clouds than the other applied cloud filters, so in the case of clouds it would screen out more pixels than the other filters) did not screen out any additional pixels, the scene is either uniformly filled with just clouds to which none of the filter are sensitive (improbable) or it is a cloud free scene. The boxes where this happens are kept and used for validation.

This method proved to be successful for the case studies on single swaths which do not undergo gridding with limitation on the minimum allowed amount of pixels. For our MERIS gridded products, the gridding procedure tends to introduce a similar cloud screening effect as the above mentioned filter. High thin clouds, however, may be still

The melt pond fraction and spectral sea ice albedo retrieval from MERIS data

L. Istomina et al.

Title Page

Abstract

Introduction

Conclusions

References

Tables

Figures

◀

▶

◀

▶

Back

Close

Full Screen / Esc

Printer-friendly Version

Interactive Discussion

The melt pond fraction and spectral sea ice albedo retrieval from MERIS data

L. Istomina et al.

Title Page

Abstract

Introduction

Conclusions

References

Tables

Figures

◀

▶

◀

▶

Back

Close

Full Screen / Esc

Printer-friendly Version

Interactive Discussion

Within this work, we apply the MPD algorithm without limitations other than cloud screening (original as described by Zege et al., 2014, and dynamic spatial filter described in Sect. 3.2.2) to illustrate the effect of the above mentioned underestimation for global applications of the algorithm (Sect. 5). In cases not dedicated to the study of the algorithm accuracy, it is recommended to use the MPD MPF product in combination with the reanalysis air surface temperature to apply the algorithm only when the melt ponds are not frozen over. Otherwise the (supposedly low) MPF value is ambiguous and could indicate both low MPF of open ponds or high MPF of frozen ponds. It is planned to resolve this ambiguity in the future versions of the algorithm by introducing a decision tree based on the air temperature as a measure of surface energy balance to determine whether ponds are frozen over or not.

Both cruises TransArc2011 (Fig. 16) and HOTRAX 2005 (Fig. 17) had only several days of cloud free collocations. The available swath data and the hourly ship observations have been compared point by point without temporal averaging. The only averaging was the 15 km spatial averaging of the satellite data around the ship location. For both cruises, information on ice concentration was available and the ship MP values have been corrected for ice concentration to give the pond fraction relative to the visible area and not to the area of sea ice. For the TransArc2011 cruise, information on MYI and FYI ice concentration was available with corresponding MPFs. The total MPF was calculated using the linear mix of these values. However, the resulting cloud free collocations feature mostly FYI cases. For the HOTRAX 2005, such information was not available and only ice concentrations were used.

3.2.4 In situ validation

The in situ validation has been performed on the swath data using the three available datasets: transect measurements on the FI just north of Barrow, AK, approximately 1 km offshore from Niksiuraq in the Chukchi sea, near 71°22' N, 156°33' W throughout June 2009 (Polashenski et al., 2012), 100 m transect and visual estimations on the 3 km × 3 km area of landfast FYI approximately 80 km northwest of Resolute Bay,

Nunavut, 75°14' N, 97°09' W, between 18 June and 10 July 2002 as part of the Collaborative Interdisciplinary Cryosphere Experiment (C-ICE) 2002 project (Scharien and Yackel, 2005), and 200 m transect fractions on landfast FYI also in the vicinity of Resolute Bay, Nunavut, 74°44' N, 95°06' W, between 26 June and 11 July 2006 (Sect. 3.1.1).

During C-ICE 2002 visual estimates of MPF fraction were made on a homogeneous and relatively smooth zone of FI in the Canadian Arctic Archipelago approximately 80 km northwest of Resolute Bay, Nunavut between 18 June 2002 and 8 July 2002 (Scharien and Yackel, 2005). Visual estimates were supported by occasional 100 m transect measurements taken at 0.5 m intervals to characterize surface feature types (melt pond or ice) and pond depths, as well as timelapse photos taken from a tower based camera mounted at 6 m height. From these data a nominal 0.1 MPF estimation error was ascribed to the visual estimates. For days where transect measurements were available, the daily average of W–E and N–S transects was used instead of visual estimates.

For the rest two datasets, the transect measurements of MPFs were used as provided.

The datasets feature uniform FI and at times of extremely high pond fractions and the following drainage events. As the campaigns were performed on the FI, no correction for the ice concentration was needed. As in case of ship cruises, the average MPF 15 km around each in situ point was taken. The same cloud filtering has been applied (original as described by Zege et al. (2014), and dynamic spatial filter described in Sect. 3.2.2). The total amount of cloud free collocated points is $N = 47$, total RMS = 14 %, total $R = 0.72$. The correlation plot for the two datasets is shown in Fig. 18.

The melt pond fraction and spectral sea ice albedo retrieval from MERIS data

L. Istomina et al.

Title Page

Abstract

Introduction

Conclusions

References

Tables

Figures

◀

▶

◀

▶

Back

Close

Full Screen / Esc

Printer-friendly Version

Interactive Discussion



4 Case studies

4.1 Gridding

The processed swath MERIS Level 1b data have been gridded daily into the 12.5 km polar stereographic grid (the so-called NSIDC grid) with the criterion of more than 50 % valid pixels (both spatially and temporally) within a grid cell to produce a valid grid cell. The SD of such a mixed spatial and temporal average is also provided. Thus, the resulting NetCDF contains four datasets: MPF, broadband albedo and their SDs. On average, there were around 13 overflights per day, with the density of overlapping swaths highest at about 80° N latitude. Even from a single overflight, there are at least 100 up to about 1000 data points for averaging into a single grid cell. Assuming a stable retrieval and low variations within a single day, the SD gives information about the variation of MPF and broadband albedo. However, since the Arctic is one of the most cloud covered region (80 % cloud covered throughout the year, Serreze and Barry, 2005) and such a method reliably screens out only cloud edges. This kind of averaging does not provide a guarantee of a valid data point for every single day and grid point.

Gridded daily products are used to produce averages of higher order, e.g. weekly averages. Here again, more than half of available pixels have to be valid numbers to obtain a valid averaged value for a given grid cell. No weight or threshold on SDs is applied. The resulting SD is then written into the resulting NetCDF file together with the averaged value for the broadband albedo and MPF.

These weekly averages have a much higher data density since there is a higher probability for the satellite to observe cloud free areas within one week than it is the case for one day.

The essential difference in daily and e.g. weekly averages is the data coverage due to cloudiness and smoothness of the resulting product.

TCD

8, 5227–5292, 2014

The melt pond fraction and spectral sea ice albedo retrieval from MERIS data

L. Istomina et al.

Title Page

Abstract

Introduction

Conclusions

References

Tables

Figures

◀

▶

◀

▶

Back

Close

Full Screen / Esc

Printer-friendly Version

Interactive Discussion



4.2 Comparison to reanalysis air temperature at the surface: time sequences of the daily gridded MPF and albedo for FYI and MYI

In order to illustrate the feasibility of the algorithm on FYI and MYI, time sequences over the summer 2009 have been produced for Beaufort Sea with mainly FY ice and North Greenland with mainly MY ice (Fig. 19).

For this study, the daily averaged product was taken in the area 75° N, 155° W (Beaufort Sea) and 84.5° N, 35° W (North Greenland) and it was compared to the time sequence of daily averaged air temperature at the surface (0.995 sigma level) from NCEP reanalysis data (Kalnay et al., 1996). The difference between melt evolution in the selected location is mainly that melt onset happens about a month earlier in lower latitudes: beginning of June on FYI as opposed to beginning of July for MYI. Then, due to MYI being much less even than FYI, the maximum MPF on FYI can be about 4 times higher than that on MYI (maximum melt 0.2 on MYI as opposed to up to 0.8 on MYI, Fig. 1). While the melt onset occurs rapidly on both ice types, the later stage of melt – drainage of melt ponds – happens much sooner on FYI than on MYI. On MYI, this stage is generally substituted with MPF decrease due to freezing and snowfalls unless the MY ice is very rotten.

One more difference between the two chosen locations is the sea ice concentration: for the MYI the ice concentration stays very high throughout the whole summer, whereas for the FYI region the effect of ice concentration and also ice drift (in the swath data for consecutive days separate floes and their drift is clearly visible) can affect the time sequence analysis, affecting the noisiness of the retrieved values.

Overall, the comparison of the retrieved MPFs and albedos to the surface air temperature (Figs. 20 and 21) shows a clear connection between these during the melt onset: as soon as air temperature assumes constantly positive values, sea ice albedo drops down and MPF increases abruptly. For both FYI and MYI the maximum MPF is around 0.35, with melt onset happening in the beginning of June for FYI and beginning of July for MYI. This corresponds to the knowledge about melt onset and dynamics from

TCD

8, 5227–5292, 2014

The melt pond fraction and spectral sea ice albedo retrieval from MERIS data

L. Istomina et al.

Title Page

Abstract

Introduction

Conclusions

References

Tables

Figures

◀

▶

◀

▶

Back

Close

Full Screen / Esc

Printer-friendly Version

Interactive Discussion

MERIS dataset. A more detailed analysis of MPF and albedo for the whole summer including their parameterization will be presented in a follow-up publication.

5.1 Weekly averages of June 2007 and 2011: how the record ice minimum in 2007 started

5 It is interesting to compare the evolution of melt right after the onset of melt for record sea ice minimum in 2007 and a similar by the ice minimum extent year 2011, to see how the patterns of melt changed within these 5 years to reach the same resulting ice extent during the sea ice minimum. In Fig. 22 the evolution of the MPFs from the last two weeks of May up to first two weeks of September 2007 and 2011 is shown. The
10 onset of melt happens in the fourth week of May at the shore of Beaufort Sea (2007) and East-Siberian Sea (2011).

The melt onset during the first week of June has much more local character in 2011 than in 2007, being centered near point Barrow and the shore of Beaufort Sea, as opposed to 2007 when the melt onset started already at a more global scale. The
15 second week of June 2007 featured drastic melt in the Beaufort Sea and the western part of the FYI covered Arctic Ocean (top row in Fig. 23), whereas in 2011 the situation was more or less stable relative to the first week of June.

In the third and the fourth weeks of June 2011 large scale melt started (third week of June 2011, one week delay as compared to June 2007), but it is centered around the
20 Queen Elizabeth Islands. The fourth week of June 2011 shows that melting spreads from there over the Eurasian Arctic Ocean, whereas in 2007 at this time these areas have already experienced the maximum of melt and are now draining. MYI areas to the north of Greenland and Queen Elizabeth Islands for both years display start of melting, which continues in July. The relatively high MPFs throughout the whole Arctic
25 Ocean are interrupted with lower air temperatures in the Eurasian Arctic in the second week of July 2007 (bottom row in Fig. 23). The lower air temperatures are evident in the time sequence of daily averaged NICEP air temperatures (0.995 sigma level) and MPFs (Fig. 24) for both years for the characteristic location in the Barents Sea,

The melt pond fraction and spectral sea ice albedo retrieval from MERIS data

L. Istomina et al.

Title Page

Abstract

Introduction

Conclusions

References

Tables

Figures

◀

▶

◀

▶

Back

Close

Full Screen / Esc

Printer-friendly Version

Interactive Discussion



The melt pond fraction and spectral sea ice albedo retrieval from MERIS data

L. Istomina et al.

Title Page

Abstract

Introduction

Conclusions

References

Tables

Figures

◀

▶

◀

▶

Back

Close

Full Screen / Esc

Printer-friendly Version

Interactive Discussion

where lower MPFs are observed in the second week of July 2007 as compared to 2011 (100 km average around 85° N, 65° E). A reference location north to the Queen Elizabeth Islands is also shown in Fig. 24 (100 km average around 83° N, 110° W). The locations of the two sites are shown with yellow square with tags “E” and “W” correspondingly in Fig. 19. The differences in the MPFs for the second week of June and second week of July 2007 and 2011 are summarized in Fig. 23.

The rest of July and first two weeks of August feature similar melt evolution with occasional freezeup and melt (Fig. 22). The frequent freezeups and snowfalls caused the MPF decrease at the northernmost latitudes in the last two weeks of August of both 2007 and 2011, while the melt ponds were still present closer to the ice edge of the Arctic ocean (also can be seen in Fig. 24). The MPF decreases overall throughout the Arctic Ocean (according to the air temperature, the ponds are frozen over and snow covered) in the first two weeks of September of both 2007 and 2011.

To conclude: the years 2007 and 2011 feature different times of melt onset and also different spatial patterns of MPFs, however the ice extent near the ice minimum is similar. The most prominent feature is the rapid and large scale melt in the second week of June 2007 which was not reproduced in 2011. This feature seems to be compensated by smaller MPFs in the first two weeks of July 2007, whereas the MPFs during the same time period in 2011 again do not reproduce this feature (Fig. 23). This kind of opposite temporal MPF dynamics (2007) produces the same effect as an evolution of melt uniform in time (2011). Analysis of MPF time sequences (Fig. 24) shows only a moderate (about 15 %) difference of MPF amplitude during the first and second week of July 2007 and 2011, but such a moderate MPF difference over a large area (Fig. 23) has a significant effect on the minimum ice extent: for both 2007 and 2011, the areas of higher MPFs during any phase of the melt evolution are ice free at the time of ice minimum (1st and 2nd weeks of September, Fig. 22).

5.2 Spatial trends of melt pond fractions for the Arctic Ocean over the whole MERIS dataset (2002–2011)

As seen from the comparison to in situ data and reanalysis temperature data, the MPD retrieval is

1. affected by unscreened high thin clouds, to which none of the available cloud filters is sensitive but which affect the retrieved MPF and albedo because clouds tend to increase the albedo/decrease pond fraction for areas of high true MPF and increase MPF/decrease albedo for areas of no or little melt. This produces an offset at the low MPFs and is mainly visible at the beginning of the melt season. It affects also the maximum reachable MPFs at the peak of the melt and the minimum MPFs before and after the season.
2. Performance of the algorithm is compromised during the end of the melt season due to the presence of overfrozen, snow covered or melted through melt ponds.

Therefore, for the future versions of the algorithm an improvement of the MERIS cloud mask over snow, potentially in synergy with another sensors like AATSR for historic MERIS dataset, would be the first priority. Moreover, the usage of additional data such as the reanalysis temperature will help to determine cases where MPD should not be applied. For sensors with available TIR and NIR channels, both disadvantages would disappear due to more reliable cloud screening and availability of surface temperature information from the same sensor.

Nevertheless, for the MERIS data the temporal dynamics of the retrieved quantities compares well with the NCEP air at the surface temperature data and the weekly averages show pronounced spatial variability of the retrieved pond fractions for different years which cannot be explained by thin cloud cover. This gives us the possibility to study the trends of the retrieved quantities as the systematic offset due to clouds would be cancelled out and only variability of the true value shows up in the trend (Fig. 25).

The melt pond fraction and spectral sea ice albedo retrieval from MERIS data

L. Istomina et al.

Title Page

Abstract

Introduction

Conclusions

References

Tables

Figures

◀

▶

◀

▶

Back

Close

Full Screen / Esc

Printer-friendly Version

Interactive Discussion



The trend significance given by the map of the MPF trend p value (Fig. 26) confirms this: the strongest positive or negative trends are most significant ones.

There is no trend for the first week of June throughout the years (Fig. 25), except for a slight positive trend of MPF near Point Barrow. This feature disappears for the second week, and a starting positive trend of 1–2 % per investigation period is located near Queen Elizabeth Islands. This trend exists for the whole month of June. Possible explanation for it is not the increased absolute value MPF, but earlier melt onset for these areas as related to the beginning of the dataset. A negative trend in the East-Siberian Sea has yet to be explained: either it is the opposite temporal shift of melt evolution towards summer, or a shift of melt evolution towards spring with e.g. drainage phase of melt observed instead of maximum melt, or a fluctuation in the weather conditions or in the ice type in the area within the studied years. It is important to understand that the trend of the MPF can as likely occur due to temporal shift of the melt process towards spring or autumn, as well as change of maximum possible pond fraction due to ice type change. The maximum and average MPFs depend not only on the air temperature, but also on the sea ice roughness of various scales and other ice properties (Polashenski et al., 2012), so an increasing air temperature trend in the area would not necessarily produce an increasing MPF trend. The time sequence of MPF for the studied years for the location of interest in the East Siberian Sea (74° N, 160° E averaged 50 km around the point) is shown in Fig. 27. The MPF curves for different years hardly show any temporal shift, but display a change of absolute MPF and of temporal behavior of the melt evolution, which is an indication of an ice type change from FYI to MYI. E.g. the curve corresponding to 2011 in Fig. 27 (red curve) shows a clear MYI MPF dynamics. The presence of the MYI in the area is confirmed by analyzing the maps of ice concentration for the autumn before in the region of interest (not shown here, for details see AMSR-E ice concentration maps provided by Uni Bremen, <http://www.iup.uni-bremen.de:8084/databrowser.html>). At the same time, a similar plot (Fig. 28) for the Queen Elizabeth Islands (50 km around 78° N, 108° W) displays the exact opposite: the peak of MPF for the melt onset shifts towards spring in the later

The melt pond fraction and spectral sea ice albedo retrieval from MERIS data

L. Istomina et al.

Title Page

Abstract

Introduction

Conclusions

References

Tables

Figures

◀

▶

◀

▶

Back

Close

Full Screen / Esc

Printer-friendly Version

Interactive Discussion



years of the MERIS dataset, whereas the absolute value of the MPF peak stays the same. This is the sign of warm atmospheric masses appearing earlier in the summer than before, producing the positive MPF trend for the area.

The MPF trend for the 4th week of June features earlier melt onset in the MYI regions and further melt overall in the Arctic ocean with occasional hints of longitudinal oscillations, e.g. in week 4 of June, Fig. 25.

5.3 Spatial trends of broadband sea ice albedo for the Arctic Ocean over the whole MERIS dataset (2002–2011)

The MPF and the broadband albedo of the pixel are joint products, i.e. increasing trend of MPF gives a decreasing trend of the albedo. Decreasing albedo trend around Queen Elizabeth Islands and increasing trend in the East-Siberian Sea (see Fig. 29) correspond well to already seen dynamics of the MPF weekly trends, with slight differences in spatial patterns which can be explained by different sensitivity of both retrievals to open water and melt ponds: MPFs are not sensitive to open water (OW), whereas the albedo of the pixel includes also OW. The albedo trend significance which displays similar spatial pattern as that of MPF is shown in Fig. 30.

6 Conclusions

Melt ponds on sea ice affect the radiative properties of the ice cover and its heat and mass balance. In order to assess the change of the energy budget in the region (e.g. with GCM), among other sea ice and melt pond properties, the sea ice reflective properties and the amount of melt ponds on sea ice have to be known. This work has validated a retrieval of MPF and broadband sea ice albedo from MERIS data (Zege et al., 2014) against aerial, in situ and ship-based observations. In addition, the retrieved MPFs and albedo values have been compared to reanalysis air surface temperatures.

The melt pond fraction and spectral sea ice albedo retrieval from MERIS data

L. Istomina et al.

Title Page

Abstract

Introduction

Conclusions

References

Tables

Figures

◀

▶

◀

▶

Back

Close

Full Screen / Esc

Printer-friendly Version

Interactive Discussion



its peak but no temporal shift, positive MPF trend around Queen Elizabeth Islands connected to the earlier melt onset but peak MPF values staying the same (Figs. 27–29). These will be analyzed further in a follow-up publication.

The presented melt pond fraction and sea ice albedo retrieval can be applied to other radiometers with a sufficient number of channels in the VIS and NIR e.g. VIIRS onboard Suomi NPP and OLCI onboard the Sentinel-3 ESA mission (planned launch 2014). This will also allow extending the algorithm validation for the data from e.g. research cruises of RV *Polarstern* after 2011, which could not be used here because of the failure of ENVISAT. These more recent ice observations have been obtained within the newer and more accurate ASSIST protocol. Thus the continuity of the MPF and sea ice albedo dataset can be achieved, which is important for the dataset use as input to GCM and for self-sufficient studies of MPF and albedo dynamics in the context of global change and Arctic amplification.

Acknowledgements. The authors express gratitude to Stefan Hendricks for providing photos of the hourly bridge observations of the TransArc2011 cruise, to Daniel Steinhage for providing photos taken with a downward-looking camera during the aircraft campaign NOGRAM-2 2011, to the C-ICE 2002 participants, J. Yackel and the Cryosphere Climate Research Group, Department of Geography, University of Calgary. The Centre for Earth Observation Science at the University of Manitoba and the Polar Continental Shelf Project are gratefully recognized for their logistic and financial support.

NCEP Reanalysis data provided by the NOAA/OAR/ESRL PSD, Boulder, Colorado, USA, from their web site at <http://www.esrl.noaa.gov/psd/>.

This work has been funded as a part of project SIDARUS under FP7-SPACE-2010-1, grant number 262922.

TCO

8, 5227–5292, 2014

The melt pond fraction and spectral sea ice albedo retrieval from MERIS data

L. Istomina et al.

Title Page

Abstract

Introduction

Conclusions

References

Tables

Figures

◀

▶

◀

▶

Back

Close

Full Screen / Esc

Printer-friendly Version

Interactive Discussion



References

- Bannehr, L. and Schwiesow, R.: A technique to account for the misalignment of pyranometers installed on aircraft, *J. Atmos. Ocean. Tech.*, 10, 774–777, doi:10.1175/1520-0426(1993)010<0774:ATTAFT>2.0.CO;2, 1993.
- 5 Birnbaum, G., Dierking, W., Hartmann, J., Lüpkes, C., Ehrlich, A., Garbrecht, T., and Sellmann, M.: The Campaign MELTEX with Research Aircraft “POLAR 5” in the Arctic in 2008, *Berichte zur Polar- und Meeresforschung/Reports Polar Mar. Res.*, 593, 3–85, 2009.
- Bricaud, A., Morel, A., and Prieur, L.: Absorption by dissolved organic matter of the sea Domains, (yellow substance) in the UV and visible, *Limnol. Oceanogr.*, 26, 43–53, 1981.
- 10 Curry, J. A., Schramm, J. L., and Ebert, E. E.: Sea-ice albedo climate feedback mechanism, *J. Climate*, 8, 240–247, 1995.
- Eicken, H., Grenfell, T. C., Perovich, D. K., Richter-Menge, J. A., and Frey, K.: Hydraulic controls of summer Arctic pack ice albedo, *J. Geophys. Res.-Oceans*, 109, C08007, doi:10.1029/2003JC001989, 2004.
- 15 Geldsetzer, T., Scharien, R. K., Yackel, J. J., Cheng, B., and Else, B. G. T.: Multipolarization SAR for Operational Sea Ice Monitoring, Technical Report for POL-ICE 2006 2006-12-11, Cryosphere Climate Research Group, Calgary, Canada, 2006.
- Gonzalez, R. C. and Woods, R. E.: *Digital Image Processing*, 2nd Edn., Prentice Hall Inc., Upper Saddle River, NJ, USA, 2002.
- 20 Grenfell, T. C. and Perovich, D. K.: Seasonal and spatial evolution of albedo in a snow-ice-land-ocean environment, *J. Geophys. Res.*, 109, C01001, doi:10.1029/2003JC001866, 2004.
- Istomina, L., Nicolaus, M., and Perovich, D.: Spectral Albedo of Sea Ice and Melt Ponds Measured During *POLARSTERN* Cruise ARK XXII/3 (IceArc) in 2012, PANGAEA Dataset, Institut für Umweltphysik, Universität Bremen, Bremen, doi:10.1594/PANGAEA.815111, 2013.
- 25 Jensen, J.: *Introductory Digital Image Processing: a Remote Sensing Perspective*, 3rd Edn., Prentice Hall Inc., Upper Saddle River, NJ, USA, 2008.
- Kalnay, E., Kanamitsu, M., Kistler, R., Collins, W., Deaven, D., Gandin, L., Iredell, M., Saha, S., White, G., Woollen, J., Zhu, Y., Leetmaa, A., Reynolds, R., Chelliah, M., Ebisuzaki, W., Higgins, W., Janowiak, J., Mo, K. C., Ropelewski, C., Wang, J., Jenne, R., and Joseph, D.: The NCEP/NCAR 40-Year Reanalysis Project, *B. Am. Meteorol. Soc.*, 77, 437–471, doi:10.1175/1520-0477(1996)077<0437:TNYRP>2.0.CO;2, 1996.
- 30

The melt pond fraction and spectral sea ice albedo retrieval from MERIS data

L. Istomina et al.

Title Page

Abstract

Introduction

Conclusions

References

Tables

Figures

◀

▶

◀

▶

Back

Close

Full Screen / Esc

Printer-friendly Version

Interactive Discussion



The melt pond fraction and spectral sea ice albedo retrieval from MERIS data

L. Istomina et al.

Title Page

Abstract

Introduction

Conclusions

References

Tables

Figures

◀

▶

◀

▶

Back

Close

Full Screen / Esc

Printer-friendly Version

Interactive Discussion



- Kokhanovsky, A. A., Budak, V. P., Cornet, C., Duan, M., Emde, C., Katsev, I. L., Klyukov, D. A., Korkin, S. V., C-Labonnote, L., Mayer, B., Min, Q., Nakajima, T., Ota, Y., Prikhach, A. S., Rozanov, V. V., Yokota, T., and Zege, E. P.: Benchmark results in vector atmospheric radiative transfer, *J. Quant. Spectrosc. Ra.*, 111, 1931–1946, doi:10.1016/j.jqsrt.2010.03.005, 2010.
- 5 Lampert, A., Maturilli, M., Ritter, C., Hoffmann, A., Stock, M., Herber, A., Birnbaum, G., Neuber, R., Dethloff, K., Orgis, T., Stone, R., Brauner, R., Kässbohrer, J., Haas, C., Makshtas, A., Sokolov, V., and Liu, P.: The Spring-Time Boundary Layer in the Central Arctic Observed during PAMARCMiP 2009, *Atmosphere (Basel)*, 3, 320–351, doi:10.3390/atmos3030320, 2012.
- 10 Lehmann, P.: Geophysikalische Messungen for Nordostgrönland, Alfred Wegener Institute for Polar and Marine Research, Bremerhaven, 2012.
- Nicolaus, M., Katlein, C., Maslanik, J. A., and Hendricks, S.: Sea Ice Conditions During the *POLARSTERN* Cruise ARK-XXVI/3 (TransArc) in 2011, Alfred Wegener Institute, Helmholtz Center for Polar and Marine Research, Bremerhaven, 2012.
- 15 Perovich, D. K.: The Optical Properties of Sea Ice, Hanover (NH, USA) US Army Cold Reg. Res. Eng. Lab. Rep. 96-1, available at: www.dtic.mil/cgi-bin/GetTRDoc?AD=ADA310586 (last access: 10 October 2014), 1996.
- Perovich, D. K., Grenfell, T. C., Light, B., Elder, B. C., Harbeck, J., Polashenski, C., Tucker, W. B., and Stelmach, C.: Transpolar observations of the morphological properties of Arctic sea ice, *J. Geophys. Res.-Oceans*, 114, C00A04, doi:10.1029/2008JC004892, 2009.
- 20 Polashenski, C.: *Attributing Change and Understanding Melt Ponds on a Seasonal Ice Cover*, Dartmouth College, Hanover, New Hampshire, 181 pp., 2011.
- Polashenski, C., Perovich, D., and Courville, Z.: The mechanisms of sea ice melt pond formation and evolution, *J. Geophys. Res.*, 117, C01001, doi:10.1029/2011JC007231, 2012.
- 25 Press, W., Teukolsky, S., Vetterling, W., and Flannery, B.: *Numerical Recipes: the Art of Scientific Computing*, Cambridge University Press, 1987.
- Rösel, A., Kaleschke, L., and Birnbaum, G.: Melt ponds on Arctic sea ice determined from MODIS satellite data using an artificial neural network, *The Cryosphere*, 6, 431–446, doi:10.5194/tc-6-431-2012, 2012.
- 30 Scharien, R. K. and Yackel, J. J.: Analysis of surface roughness and morphology of first-year sea ice melt ponds: implications for microwave scattering, *IEEE T. Geosci. Remote*, 43, 2927–2939, 2005.

The melt pond fraction and spectral sea ice albedo retrieval from MERIS data

L. Istomina et al.

Title Page

Abstract

Introduction

Conclusions

References

Tables

Figures

◀

▶

◀

▶

Back

Close

Full Screen / Esc

Printer-friendly Version

Interactive Discussion



Scharien, R. K., Yackel, J. J., Barber, D. G., Asplin, M., Gupta, M., and Isleifson, D.: Geophysical controls on C band polarimetric backscatter from melt pond covered Arctic first-year sea ice: assessment using high-resolution scatterometry, *J. Geophys. Res.-Oceans*, 117, C00G18, doi:10.1029/2011JC007353, 2012.

5 Schlundt, C., Kokhanovsky, A. A., von Hoyningen-Huene, W., Dinter, T., Istomina, L., and Burrows, J. P.: Synergetic cloud fraction determination for SCIAMACHY using MERIS, *Atmos. Meas. Tech.*, 4, 319–337, doi:10.5194/amt-4-319-2011, 2011.

Schröder, D., Feltham, D. L., Flocco, D., and Tsamados, M.: September Arctic sea-ice minimum predicted by spring melt-pond fraction, *Nat. Clim. Change*, 4, 353–357, doi:10.1038/NCLIMATE2203, 2014.

Schwarz, P.: Quantitative Characterisation of Sea Ice Melt Stages in the Arctic by Means of Airborne Photographs, University of Trier, Trier, 114 pp., 2013.

Serreze, M. C. and Barry, R. G.: *The Arctic Climate System*, Cambridge University Press, Cambridge, 2005.

15 Shindell, D. and Faluvegi, G.: Climate response to regional radiative forcing during the twentieth century, *Nat. Geosci.*, 2, 294–300, doi:10.1038/ngeo473, 2009.

Tschudi, M. A., Maslanik, J. A., and Perovich, D. K.: Derivation of melt pond coverage on Arctic sea ice using MODIS observations, *Remote Sens. Environ.*, 112, 2605–2614, doi:10.1016/j.rse.2007.12.009, 2008.

20 Tynes, H. H., Kattawar, G. W., Zege, E. P., Katsev, I. L., Prikhach, A. S., and Chaikovskaya, L. I.: Monte Carlo and multicomponent approximation methods for vector radiative transfer by use of effective Mueller Matrix calculations, *Appl. Optics*, 40, 400–412, doi:10.1364/AO.40.000400, 2001.

Warren, S. G. and Brandt, R. E.: Optical constants of ice from the ultraviolet to the microwave: a revised compilation, *J. Geophys. Res.-Atmos.*, 113, D14220, doi:10.1029/2007JD009744, 2008.

Zege, E. P., Ivanov, A. P., and Katsev, I. L.: *Image Transfer through a Scattering Medium*, Springer-Verlag, Heidelberg, 1991.

30 Zege, E. P., Malinka, A. V., Katsev, I. L., Prikhach, A. S., Heygster, G., and Istomina, L. G.: Algorithm to retrieve the melt pond fraction and the spectral albedo of Arctic summer ice from optical data, *Remote Sens. Environ.*, in review, 2014.

The melt pond fraction and spectral sea ice albedo retrieval from MERIS data

L. Istomina et al.

Title Page

Abstract

Introduction

Conclusions

References

Tables

Figures

◀

▶

◀

▶

Back

Close

Full Screen / Esc

Printer-friendly Version

Interactive Discussion

Table 1. Datasets used for validation of the MPD algorithm.

Campaign and year	Method	Ref.
Barrow 2009	In situ field campaign, fractions along a 200 m transect	Polashenski (2011)
MELTEX 2008	Airborne measurements, supervised classification algorithm applied to geolocated quality assured aerial images	Birnbaum et al. (2009); Schwarz (2013)
NOGRAM-2 2011	Airborne measurements, supervised classification algorithm applied to geolocated quality assured aerial images	Lehmann (2012); Schwarz (2013)
C-ICE 2002	In situ field campaign, visual estimation and fractions along 100 m transects	Scharien and Yackel (2005)
HOTRAX 2005	Ship cruise, hourly bridge observations, visual estimation	Perovich et al. (2009)
TransArc 2011	Ship cruise, hourly bridge observations, visual estimation	Nicolaus et al. (2012)
POL-ICE 2006	In situ field campaign, fractions along a 200 m transect	R. Scharien, Sect. 3.1.1

The melt pond fraction and spectral sea ice albedo retrieval from MERIS data

L. Istomina et al.

Table 2. Transect measurements of surface type fractions in the Canadian Arctic, POL-ICE 2006, where the relative surface type fractions are as follows: f_1 is the snow/bare ice, f_2 – melt pond, f_3 – mixed cover, f_4 – overfrozen melt pond.

id	date_ut	time_ut	loc_y	loc_x	n	f_1	f_2	f_3	f_4
1	26 Jun 2006	15:00	74.73324	-95.10583	383	0.37	0.31	0.32	0.00
2	27 Jun 2006	0:00	74.732	-95.10324	400	0.23	0.41	0.36	0.00
3	28 Jun 2006	0:00	74.73164	-95.14458	395	0.21	0.57	0.22	0.00
4	28 Jun 2006	18:30	74.73079	-95.14778	401	0.24	0.54	0.22	0.00
5	2 Jul 2006	15:00	74.73015	-95.16151	398	0.35	0.26	0.39	0.00
6	4 Jul 2006	17:30	74.73102	-95.15971	400	0.37	0.31	0.32	0.00
7	5 Jul 2006	14:45	74.7304	-95.17052	400	0.24	0.41	0.35	0.00
8	6 Jul 2006	3:00	74.73097	-95.1729	400	0.22	0.41	0.38	0.00
9	6 Jul 2006	17:00	74.7309	-95.17329	400	0.31	0.30	0.40	0.00
10	9 Jul 2006	15:00	74.72987	-95.17271	400	0.38	0.06	0.38	0.19
11	10 Jul 2006	0:30	74.7301	-95.17448	400	0.30	0.09	0.61	0.00
12	11 Jul 2006	16:45	74.72998	-95.16605	400	0.33	0.22	0.46	0.00

Title Page

Abstract

Introduction

Conclusions

References

Tables

Figures

◀

▶

◀

▶

Back

Close

Full Screen / Esc

Printer-friendly Version

Interactive Discussion

The melt pond fraction and spectral sea ice albedo retrieval from MERIS data

L. Istomina et al.

Table 3. Integrated (320–950 nm) albedo for various surface types and total obtained from transect radiance measurements in Canadian Arctic, POL-ICE 2006, vs. corresponding retrieved broadband (400–900 nm) albedo averaged within 5 km around the location. n is the amount of measurements, f is the surface type fraction, α is the integrated albedo.

id	SNOW				MIXED				POND				Total α / retrieved
	n	f	avg α	SD α	n	f	avg α	SD α	n	f	avg α	SD α	
2	83	0.21	0.51	0.07	86	0.22	0.31	0.05	226	0.57	0.24	0.03	0.31 /NaN
3	94	0.24	0.62	0.06	89	0.22	0.40	0.13	217	0.54	0.23	0.02	0.36 /0.47
6	149	0.37	0.57	0.05	126	0.32	0.33	0.10	125	0.31	0.22	0.03	0.38 /NaN
7	97	0.24	0.54	0.05	140	0.35	0.29	0.10	163	0.41	0.21	0.02	0.32 /0.40
9	122	0.31	0.58	0.04	158	0.40	0.32	0.11	120	0.30	0.20	0.01	0.36 /0.58
10	150	0.38	0.68	0.04	152	0.38	0.38	0.12	23	0.06	0.20	0.01	0.46 /0.48
11	119	0.30	0.56	0.04	244	0.61	0.30	0.11	37	0.09	0.18	0.01	0.37 /NaN
12	132	0.33	0.71	0.07	182	0.46	0.33	0.16	86	0.22	0.20	0.02	0.43 /NaN
Combined			0.60	0.08			0.33	0.12			0.21	0.03	

Title Page

Abstract

Introduction

Conclusions

References

Tables

Figures

◀

▶

◀

▶

Back

Close

Full Screen / Esc

Printer-friendly Version

Interactive Discussion

The melt pond fraction and spectral sea ice albedo retrieval from MERIS data

L. Istomina et al.

Table 4. UTC time of aerial measurements (mpf and alb) and satellite overflights (sat) for each day of available aerial measurements of MELTEX 2008 and NOGRAM 2011.

Date	26 May 2008	3 Jun 2008	4 Jun 2008	6 Jun 2008	7 Jun 2008	21 Jul 2011
alb	20:45–21:48	17:00–19:46	19:14–23:24	no drift,	17:08–20:17	no drift,
mpf	20:55–22:55	16:59–17:53	19:14–22:03	FI	17:56–19:22	MYI
sat	20:46	19:54	21:02		21:08	

Title Page

Abstract

Introduction

Conclusions

References

Tables

Figures

◀

▶

◀

▶

Back

Close

Full Screen / Esc

Printer-friendly Version

Interactive Discussion

The melt pond fraction and spectral sea ice albedo retrieval from MERIS data

L. Istomina et al.

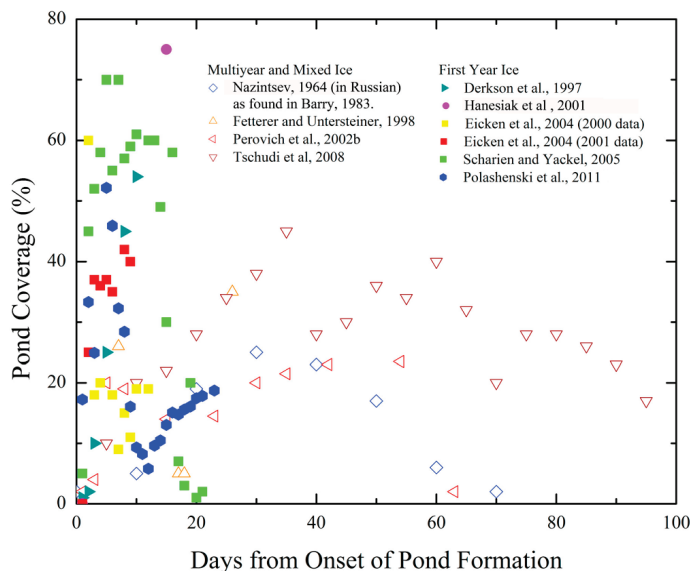


Figure 1. Pond coverage taken from various field campaigns (see legend) vs. days from onset of ponding on first year ice (filled dots) and multiyear ice (empty dots). Melt onset proceeds rapidly to the MPF maximum on FYI with following pond drainage and moderate MPFs afterwards; on multiyear ice, the evolution of melt up to the melt maximum takes longer, the peak MPF value is lower and the MPF decrease is slower than that on FYI. Figure courtesy C. Polashenski.

Title Page	
Abstract	Introduction
Conclusions	References
Tables	Figures
◀	▶
◀	▶
Back	Close
Full Screen / Esc	
Printer-friendly Version	
Interactive Discussion	



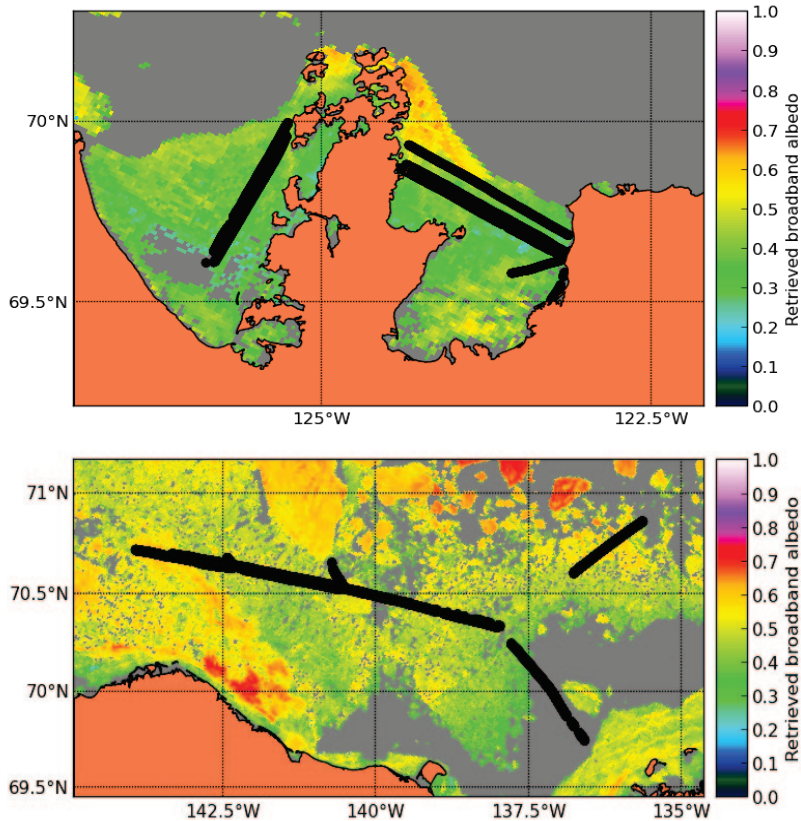


Figure 3. Examples of ice conditions present during MELTEX 2008 flights over landfast ice on 6 June 2008 (top panel) and over separate ice floes of various sizes on 4 June 2008 (bottom panel). The black tracks depict the flight tracks with albedo measurements. The color code illustrates the satellite retrieved broadband albedo. The background consists of the coral filled landmask and grey filled data gaps due to cloud contamination or surface type other than sea ice.

The melt pond fraction and spectral sea ice albedo retrieval from MERIS data

L. Istomina et al.

Title Page	
Abstract	Introduction
Conclusions	References
Tables	Figures
◀	▶
◀	▶
Back	Close
Full Screen / Esc	
Printer-friendly Version	
Interactive Discussion	



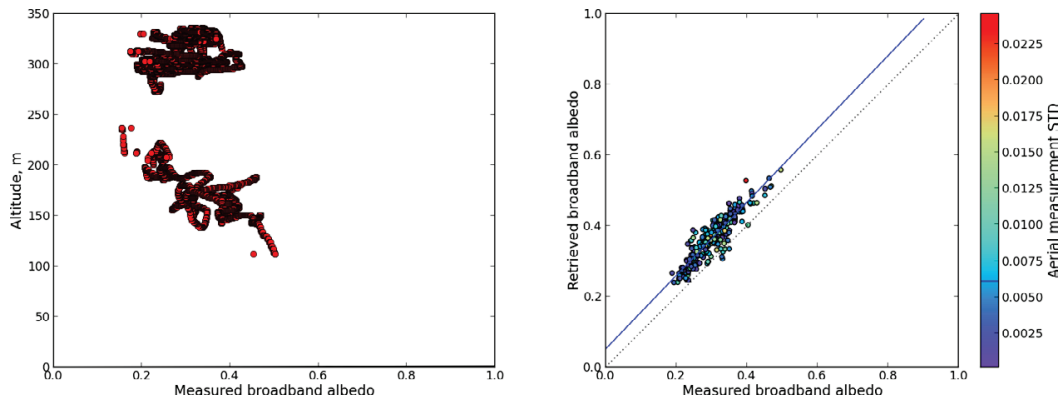


Figure 4. Altitude of the airborne broadband albedo measurements on 6 June 2008 (left). Correlation between retrieved broadband albedo from satellite data and measured broadband albedo over landfast ice (no drift) (flight track shown on the top panel Fig. 3). $N = 169$, $R = 0.917$, $RMS = 0.068$.

The melt pond fraction and spectral sea ice albedo retrieval from MERIS data

L. Istomina et al.

Title Page	
Abstract	Introduction
Conclusions	References
Tables	Figures
◀	▶
◀	▶
Back	Close
Full Screen / Esc	
Printer-friendly Version	
Interactive Discussion	



The melt pond fraction and spectral sea ice albedo retrieval from MERIS data

L. Istomina et al.

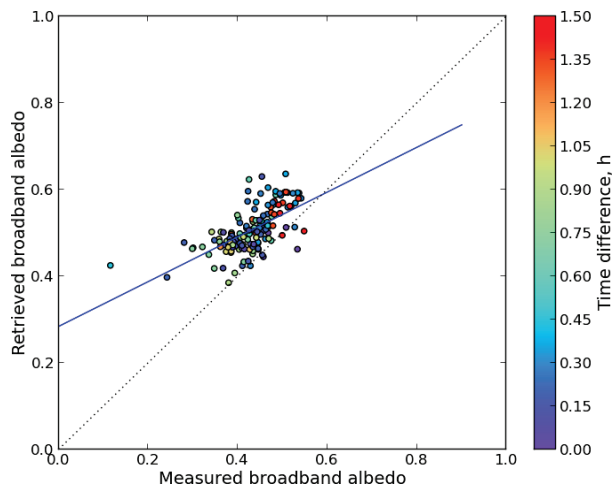


Figure 5. Correlation between broadband albedo retrieved from airborne measurements and from a satellite overflight, respectively, for the 4 June 2008 (bottom panel of Fig. 3) with respect to time difference. $N = 147$, $R = 0.622$, $RMS = 0.089$.

[Title Page](#)[Abstract](#)[Introduction](#)[Conclusions](#)[References](#)[Tables](#)[Figures](#)[◀](#)[▶](#)[◀](#)[▶](#)[Back](#)[Close](#)[Full Screen / Esc](#)[Printer-friendly Version](#)[Interactive Discussion](#)

The melt pond fraction and spectral sea ice albedo retrieval from MERIS data

L. Istomina et al.

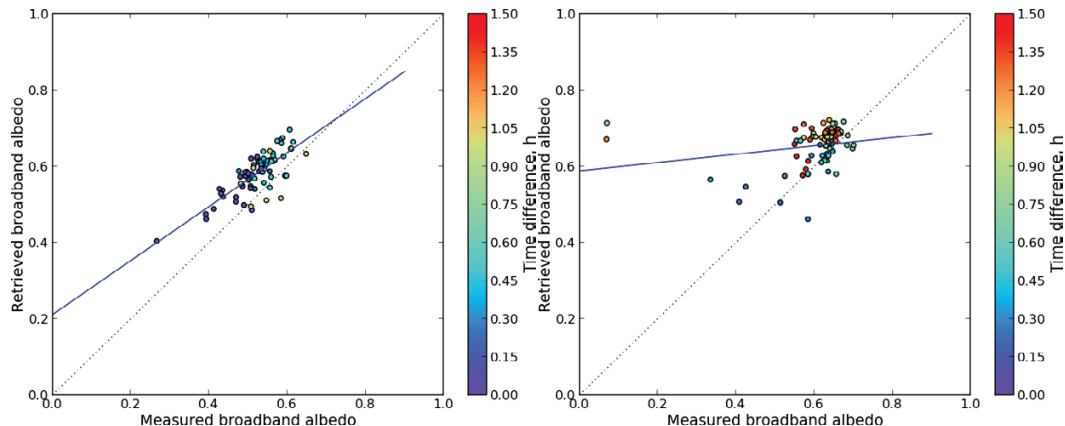


Figure 6. Correlation between broadband albedo retrieved from airborne measurements and from a satellite overflight, respectively, for the 26 May 2008 (left panel), $N = 73$, $R = 0.778$, $RMS = 0.07$ and 3 June 2008, (right panel), $N = 78$, $R = 0.22$, $RMS = 0.121$, with respect to time difference. The flight on 3 June 2008 features the greatest time difference to the satellite overflight, therefore most of the points have been discarded due to possible drift contamination.

[Title Page](#)[Abstract](#)[Introduction](#)[Conclusions](#)[References](#)[Tables](#)[Figures](#)[◀](#)[▶](#)[◀](#)[▶](#)[Back](#)[Close](#)[Full Screen / Esc](#)[Printer-friendly Version](#)[Interactive Discussion](#)

The melt pond fraction and spectral sea ice albedo retrieval from MERIS data

L. Istomina et al.

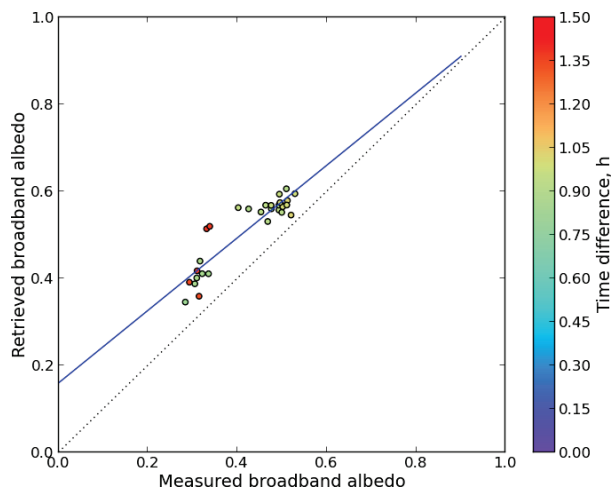


Figure 7. Correlation between broadband albedo retrieved from airborne measurements and from a satellite overflight, respectively, for the 7 June 2008, with respect to the time difference. $N = 30$, $R = 0.907$, $RMS = 0.096$.

[Title Page](#)[Abstract](#)[Introduction](#)[Conclusions](#)[References](#)[Tables](#)[Figures](#)[◀](#)[▶](#)[◀](#)[▶](#)[Back](#)[Close](#)[Full Screen / Esc](#)[Printer-friendly Version](#)[Interactive Discussion](#)

TCD

8, 5227–5292, 2014

The melt pond fraction and spectral sea ice albedo retrieval from MERIS data

L. Istomina et al.

Title Page

Abstract

Introduction

Conclusions

References

Tables

Figures

◀

▶

◀

▶

Back

Close

Full Screen / Esc

Printer-friendly Version

Interactive Discussion

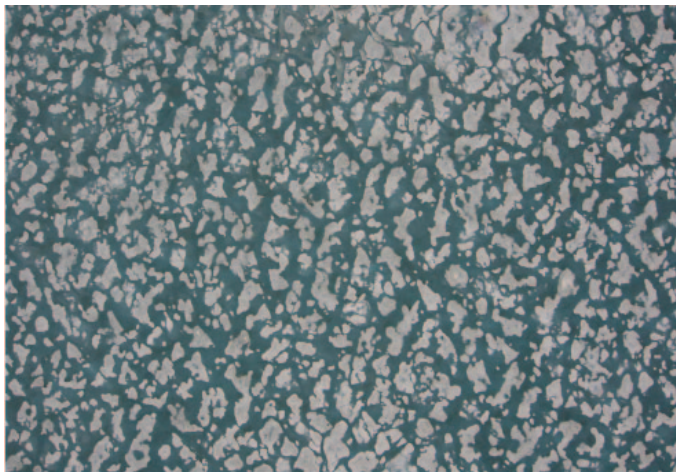


Figure 8. Example of aerial photo from MELTEX 2008 campaign, flight over landfast ice on 4 June 2008. Only quality assessed images were taken (see text for details).

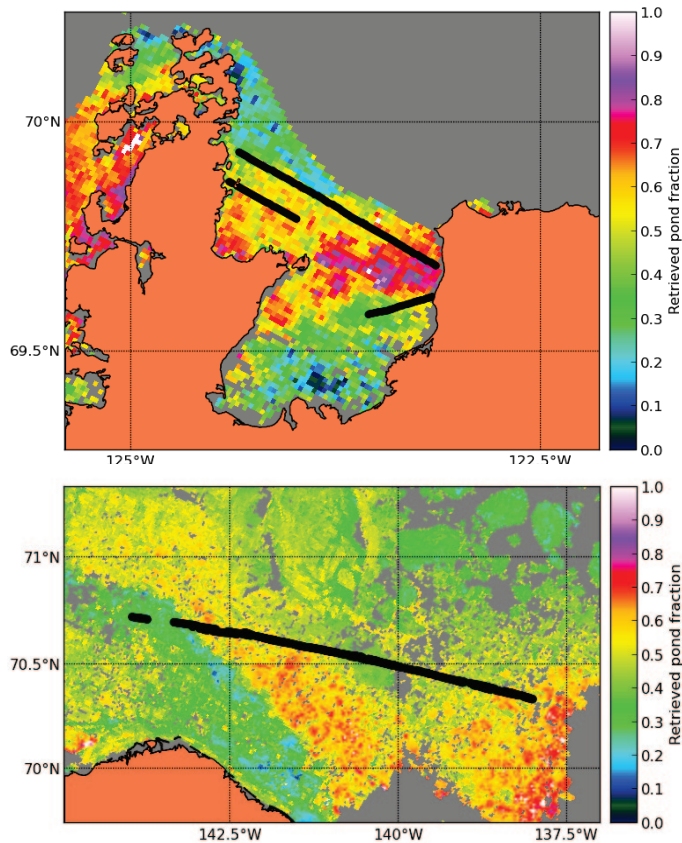


Figure 9. Examples of ice conditions present during MELTEX 2008 flights over landfast ice on 6 June 2008 (top panel) and over separate ice floes of various sizes on 4 June 2008 (bottom panel). Black dots: the flight track. The colored filled background: the satellite retrieved melt pond fraction. The background is the coral filled landmask and grey filled data gaps due to cloud contamination or surface type other than sea ice.

The melt pond fraction and spectral sea ice albedo retrieval from MERIS data

L. Istomina et al.

Title Page	
Abstract	Introduction
Conclusions	References
Tables	Figures
◀	▶
◀	▶
Back	Close
Full Screen / Esc	
Printer-friendly Version	
Interactive Discussion	



The melt pond fraction and spectral sea ice albedo retrieval from MERIS data

L. Istomina et al.

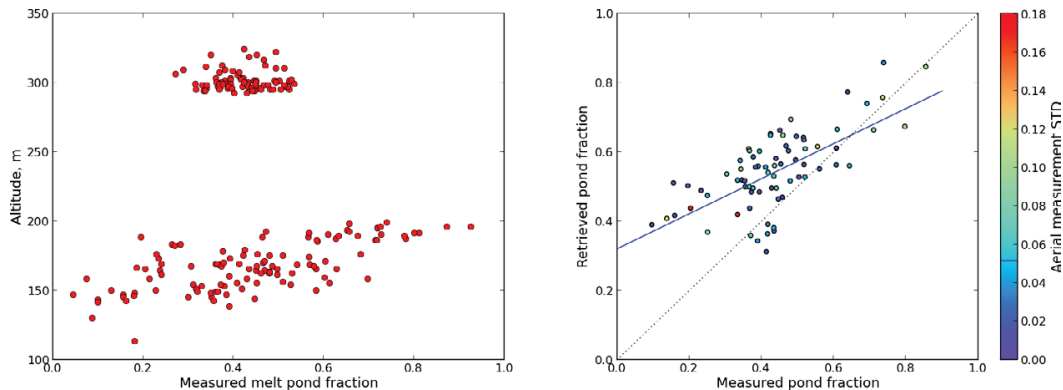


Figure 10. Altitude of the airborne melt pond measurements on 6 June 2008 (left panel). Correlation between retrieved melt pond fractions from satellite and airborne classified MP over landfast ice with no drift (right panel). The flight track shown on the top panel Fig. 9. $N = 48$, $R = 0.598$, $RMS = 0.154$.

[Title Page](#)[Abstract](#)[Introduction](#)[Conclusions](#)[References](#)[Tables](#)[Figures](#)[◀](#)[▶](#)[◀](#)[▶](#)[Back](#)[Close](#)[Full Screen / Esc](#)[Printer-friendly Version](#)[Interactive Discussion](#)

The melt pond fraction and spectral sea ice albedo retrieval from MERIS data

L. Istomina et al.

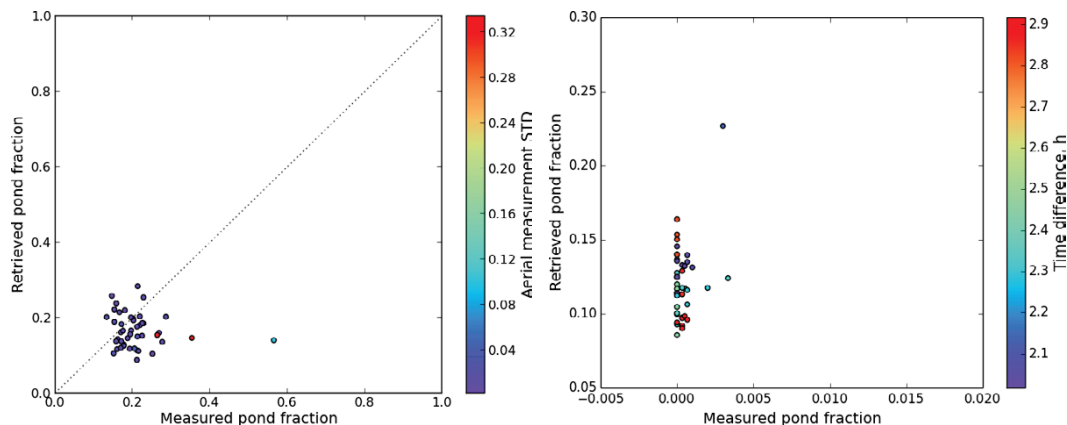


Figure 11. Correlation between retrieved melt pond fractions from satellite and airborne classified MP over MYI (no drift, ice pack), 21 November 2011, NOGRAM-2, 2011, campaign north of Greenland (left panel). $N = 40$, $R = -0.061$. RMS = 0.065 and over FYI, 3 June 2008, MELTEX 2008 (large floes but drift + large time difference) (right panel), $N = 44$, $R = 0.36$, RMS = 0.123.

The melt pond fraction and spectral sea ice albedo retrieval from MERIS data

L. Istomina et al.

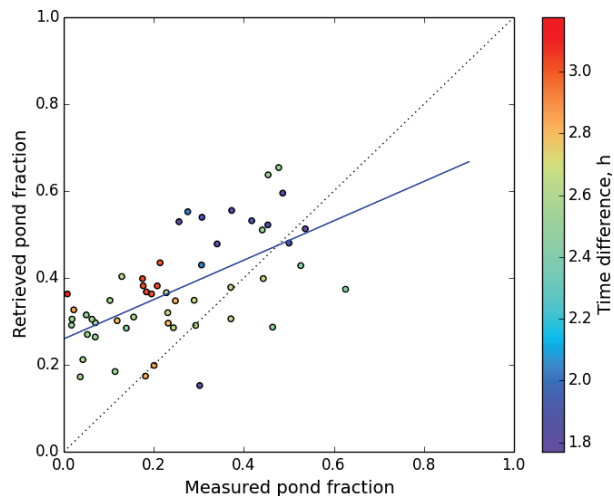


Figure 12. Correlation between retrieved melt pond fractions from satellite and airborne classified MP over FYI, possible drift, 7 June 2008, MELTEX2008 Beaufort Sea. This case features larger ice floes than flights on 4 June or 26 May 2008. $N = 53$, $R = 0.609$, $RMS = 0.179$.

Title Page

Abstract

Introduction

Conclusions

References

Tables

Figures

◀

▶

◀

▶

Back

Close

Full Screen / Esc

Printer-friendly Version

Interactive Discussion

The melt pond fraction and spectral sea ice albedo retrieval from MERIS data

L. Istomina et al.

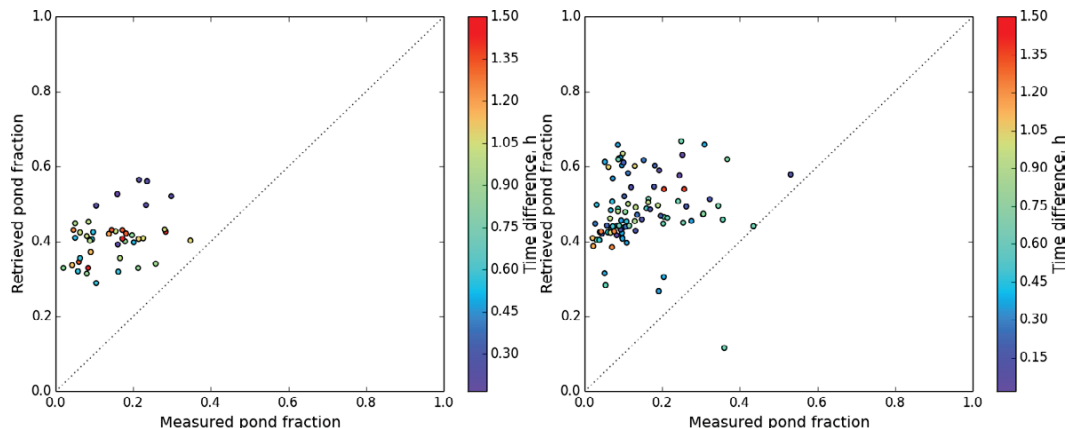


Figure 13. Retrieved melt pond fractions from satellite vs. airborne classified MP over FYI, possible drift, 26 May 2008 (left panel), $N = 44$, $R = 0.357$, $RMS = 0.274$, and 4 June 2008 (right panel, the flight track is shown in Fig. 9, bottom panel), Beaufort Sea, $N = 93$, $R = 0.143$. $RMS = 0.361$. Both cases feature extremely thrashed ice with subpixel ice floes which are covered not with white ice, but with blue ice (sea ice without the scattering layer), which has spectral response similar to MP within the VIS and IR spectral range.

Title Page	
Abstract	Introduction
Conclusions	References
Tables	Figures
◀	▶
◀	▶
Back	Close
Full Screen / Esc	
Printer-friendly Version	
Interactive Discussion	



The melt pond fraction and spectral sea ice albedo retrieval from MERIS data

L. Istomina et al.

Title Page

Abstract

Introduction

Conclusions

References

Tables

Figures

◀

▶

◀

▶

Back

Close

Full Screen / Esc

Printer-friendly Version

Interactive Discussion

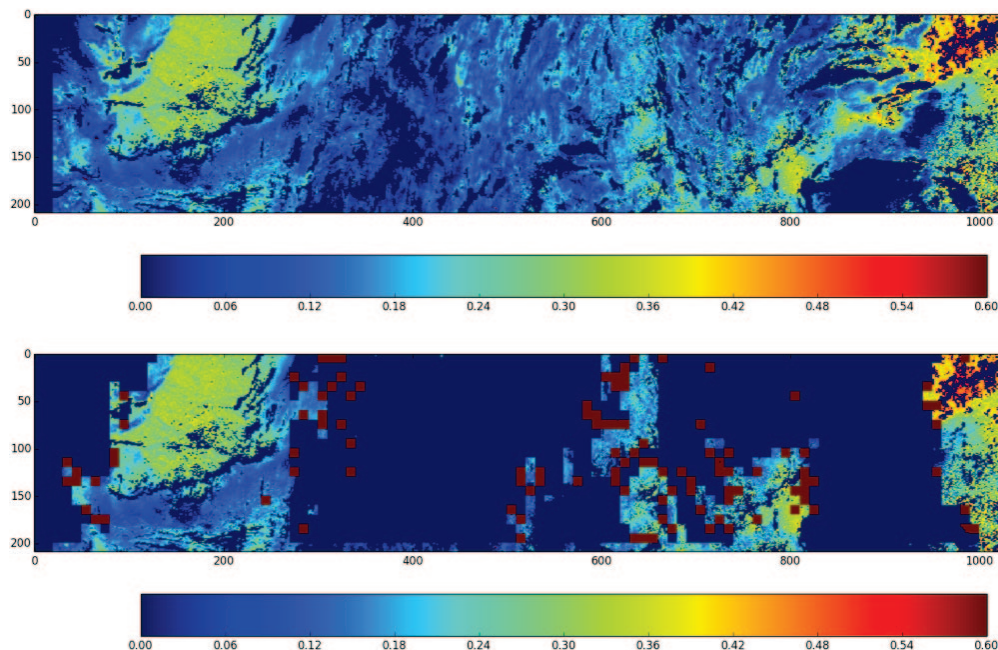


Figure 14. Example of a spatial dynamic cloud filtering for MERIS swath data: original swath subset with the cloud filters from (Zege et al., 2014) applied (top panel), same swath subset after applying the dynamic spatial filter (see text). Red boxes depict areas on the edge of the filter performance.



Figure 15. An example image made from the bridge of RV *Polarstern* during the TransArc 2011 (ARK XXVI3) on the 4 September 2011 within the course of ASPeCT observations. The estimated pond fraction is 0.5. The retrieved pond fraction for such cases will be significantly smaller. Image source Nicolaus et al. (2012).

The melt pond fraction and spectral sea ice albedo retrieval from MERIS data

L. Istomina et al.

Title Page

Abstract

Introduction

Conclusions

References

Tables

Figures

◀

▶

◀

▶

Back

Close

Full Screen / Esc

Printer-friendly Version

Interactive Discussion



The melt pond fraction and spectral sea ice albedo retrieval from MERIS data

L. Istomina et al.

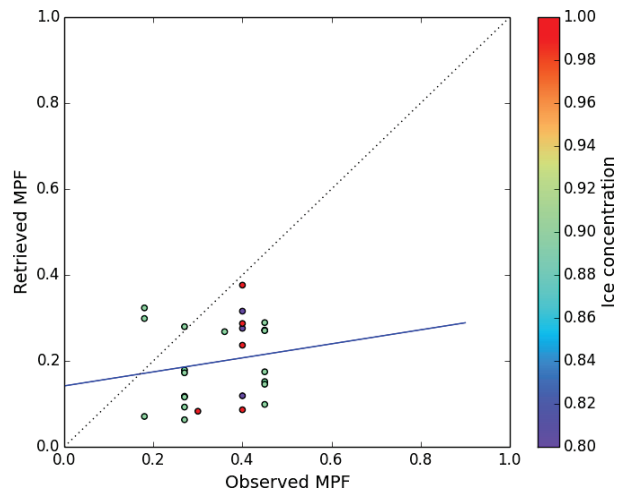


Figure 16. Retrieved MPF vs. observed MPF from the hourly bridge observations during TransArc2011, 4 August 2011–6 October 2011. Swath data, no temporal averaging, 15 km satellite average around the in situ point. All but one point is FYI. Corrected for ice concentration. Underestimation may be connected to undocumented presence of melted through or overfrozen ponds at the end of the melt season (see Fig. 15). $R = 0.162$, $RMS = 0.19$, $N = 26$.

[Title Page](#)[Abstract](#)[Introduction](#)[Conclusions](#)[References](#)[Tables](#)[Figures](#)[◀](#)[▶](#)[◀](#)[▶](#)[Back](#)[Close](#)[Full Screen / Esc](#)[Printer-friendly Version](#)[Interactive Discussion](#)

The melt pond fraction and spectral sea ice albedo retrieval from MERIS data

L. Istomina et al.

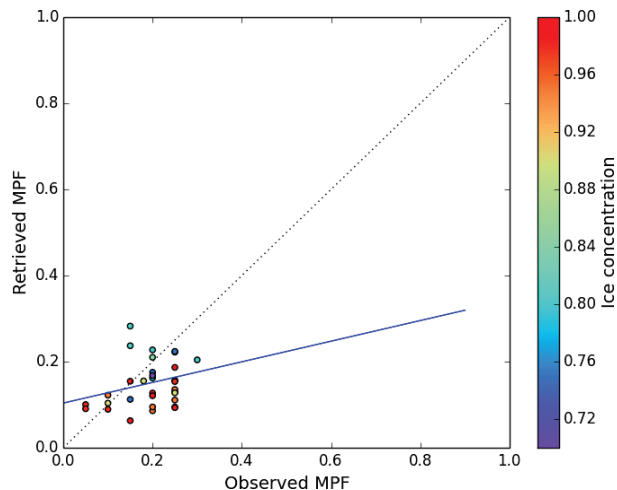


Figure 17. Retrieved MPF vs. observed MPF from the hourly bridge observations during HO-TRAX2005, 19 August–27 September 2005. Swath data, no temporal averaging, 15 km satellite average around the in situ point. No information on ice type. Corrected for ice concentration. Underestimation may be connected to undocumented presence of melted through or frozen over ponds at the end of the melt season. $R = 0.259$, $RMS = 0.084$, $N = 32$.

Title Page

Abstract

Introduction

Conclusions

References

Tables

Figures

◀

▶

◀

▶

Back

Close

Full Screen / Esc

Printer-friendly Version

Interactive Discussion

The melt pond fraction and spectral sea ice albedo retrieval from MERIS data

L. Istomina et al.

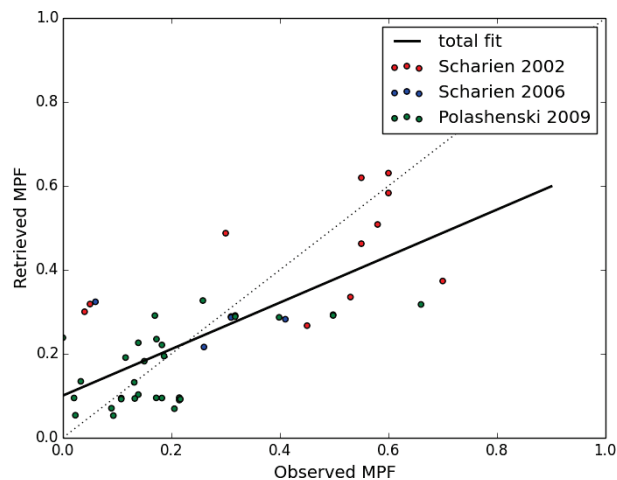


Figure 18. Three in situ campaigns on landfast ice: Scharien 2002 (red dots), Scharien 2006 (blue dots) and Polashenski 2009 (green dots). Total point number $N = 47$, $RMS = 0.14$, $R = 0.72$. The overestimation of the low MPF may be connected to unscreened thin clouds which depending on the illumination-observation geometry may appear darker than the ice and therefore cause higher retrieved MPF.

The melt pond fraction and spectral sea ice albedo retrieval from MERIS data

L. Istomina et al.

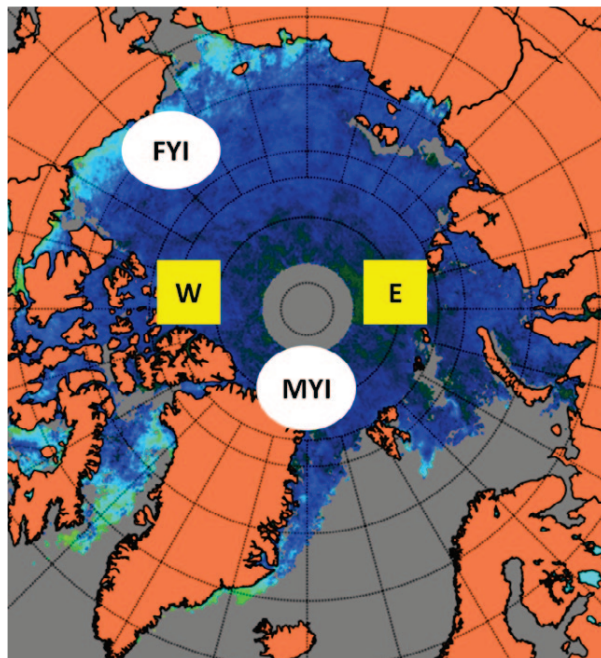


Figure 19. White circles depict locations for the time sequence analysis in summer 2009, in the Beaufort Sea, FYI (Fig. 20) and North Greenland, MYI (Fig. 21). Yellow squares show locations for two sites in both 2007 and 2011, namely in Barents Sea (E) and north to the Queen Elizabeth Islands (W) (see Fig. 24).

[Title Page](#)[Abstract](#)[Introduction](#)[Conclusions](#)[References](#)[Tables](#)[Figures](#)[◀](#)[▶](#)[◀](#)[▶](#)[Back](#)[Close](#)[Full Screen / Esc](#)[Printer-friendly Version](#)[Interactive Discussion](#)

The melt pond fraction and spectral sea ice albedo retrieval from MERIS data

L. Istomina et al.

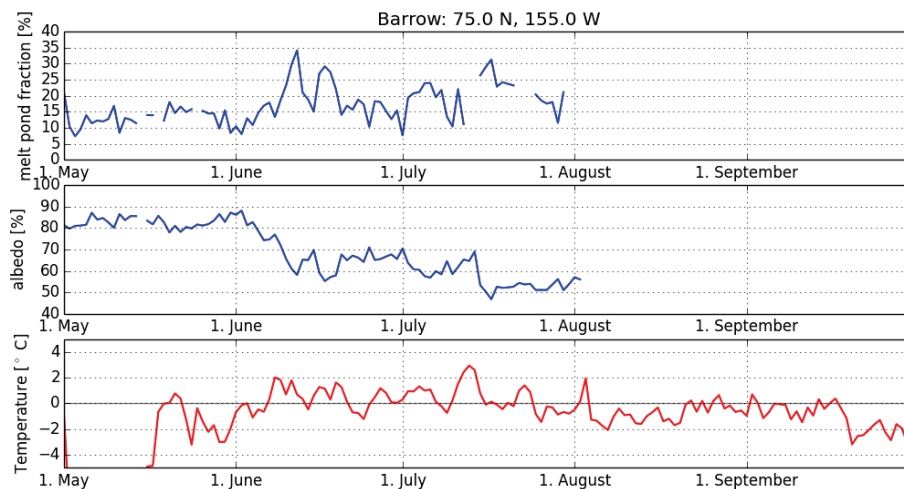


Figure 20. Time sequence of melt pond fraction, broadband albedo and NCEP air temperature at the surface for FYI area in Beaufort Sea near Barrow, May to September 2009. The albedo and MPF curves are interrupted as the area becomes completely ice free on the 1 August 2009. Location is shown in Fig. 19 with a white circle tagged “FYI”.

Title Page

Abstract

Introduction

Conclusions

References

Tables

Figures

◀

▶

◀

▶

Back

Close

Full Screen / Esc

Printer-friendly Version

Interactive Discussion

The melt pond fraction and spectral sea ice albedo retrieval from MERIS data

L. Istomina et al.

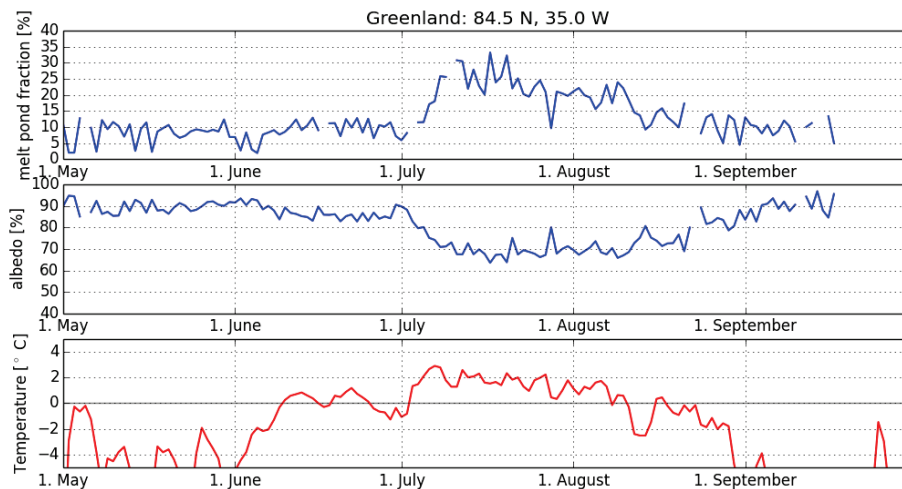


Figure 21. Time sequence of melt pond fraction, broadband albedo and NCEP air temperature at the surface for the MYI area around North Greenland, May to September 2009. Location is shown in Fig. 19 with a white circle tagged “MYI”.

Title Page

Abstract

Introduction

Conclusions

References

Tables

Figures

◀

▶

◀

▶

Back

Close

Full Screen / Esc

Printer-friendly Version

Interactive Discussion

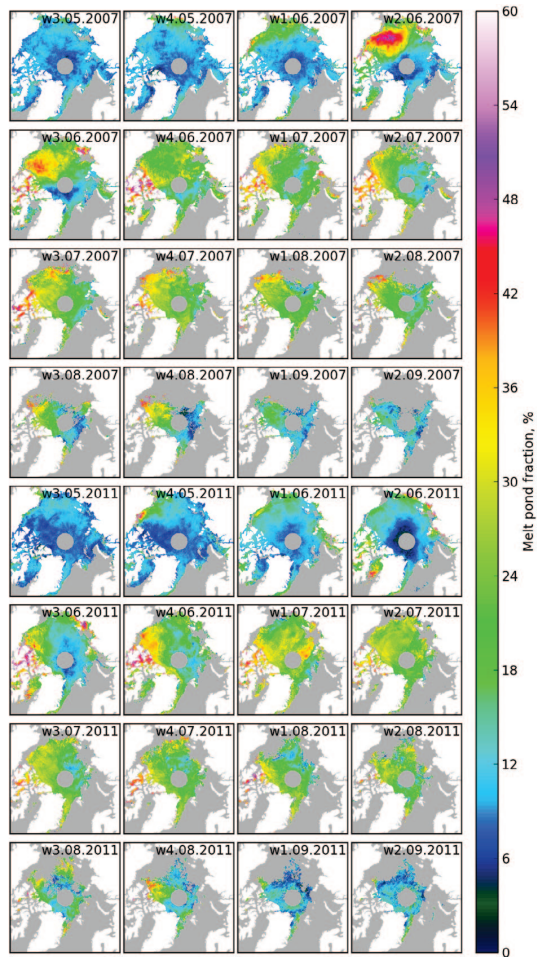


Figure 22. Retrieved weekly averaged MPF for summer 2007 and 2011.

The melt pond fraction and spectral sea ice albedo retrieval from MERIS data

L. Istomina et al.

Title Page

Abstract Introduction

Conclusions References

Tables Figures

◀ ▶

◀ ▶

Back Close

Full Screen / Esc

Printer-friendly Version

Interactive Discussion



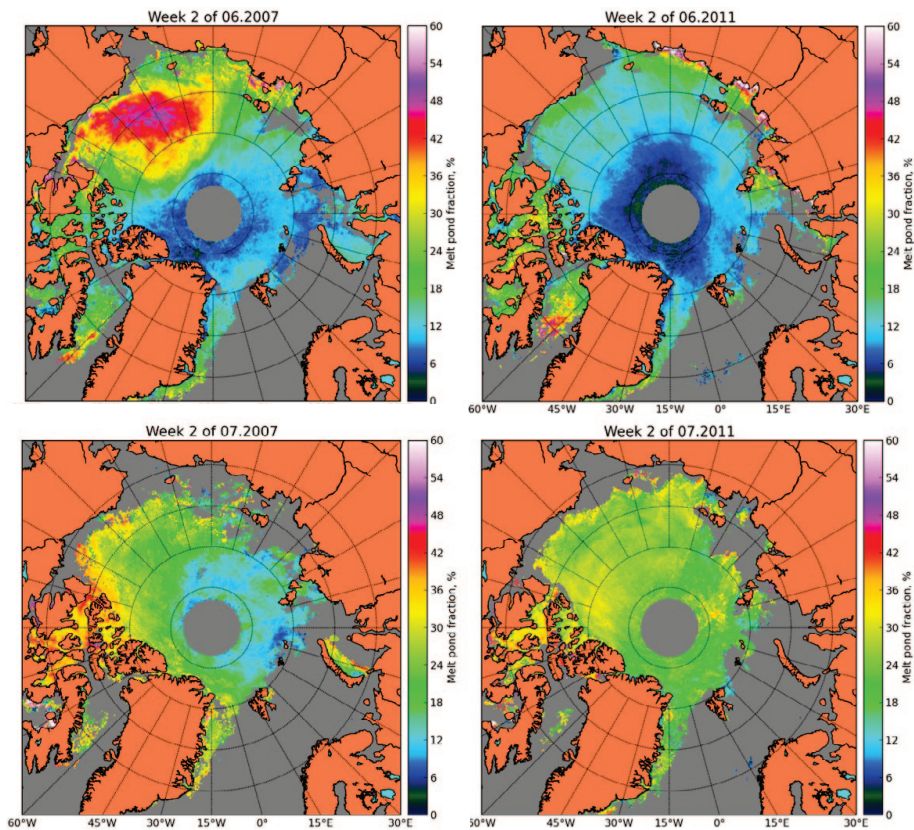


Figure 23. Main differences of weekly averages 2007 and 2011 (Fig. 22). Comparison of the weekly average pond fraction for the second week of June 2007 and 2011 (top row, left and right correspondingly) and for the second week of July 2007 and 2011 (bottom row, left and right correspondingly). Note the drastic melt onset in the 2nd week of June 2007, but lower MPFs in the 2nd week of July 2007 compared to 2011.

The melt pond fraction and spectral sea ice albedo retrieval from MERIS data

L. Istomina et al.

Title Page	
Abstract	Introduction
Conclusions	References
Tables	Figures
◀	▶
◀	▶
Back	Close
Full Screen / Esc	
Printer-friendly Version	
Interactive Discussion	



The melt pond fraction and spectral sea ice albedo retrieval from MERIS data

L. Istomina et al.

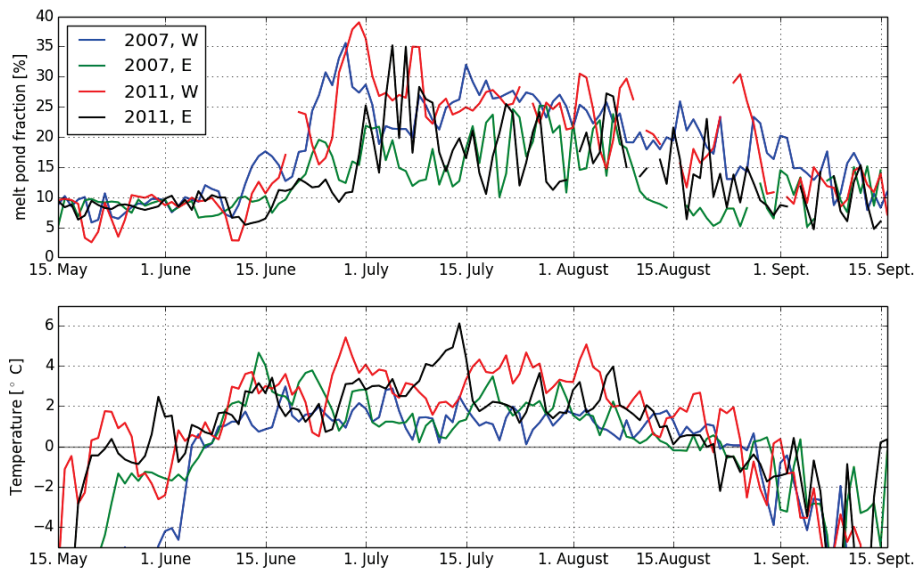


Figure 24. Daily averages of MPF (top panel) and NCEP air temperature at the surface (bottom panel) for two locations: north to the Queen Elizabeth Islands, 83° N, 110° W (tag “W” in the legend), 2007 (blue curves) and 2011 (red curves) and in the Barents Sea, 85° N, 65° E (tag “E” in the legend), 2007 (green curves) and 2011 (black curves). Locations shown in Fig. 19.

[Title Page](#)[Abstract](#)[Introduction](#)[Conclusions](#)[References](#)[Tables](#)[Figures](#)[◀](#)[▶](#)[◀](#)[▶](#)[Back](#)[Close](#)[Full Screen / Esc](#)[Printer-friendly Version](#)[Interactive Discussion](#)

The melt pond fraction and spectral sea ice albedo retrieval from MERIS data

L. Istomina et al.

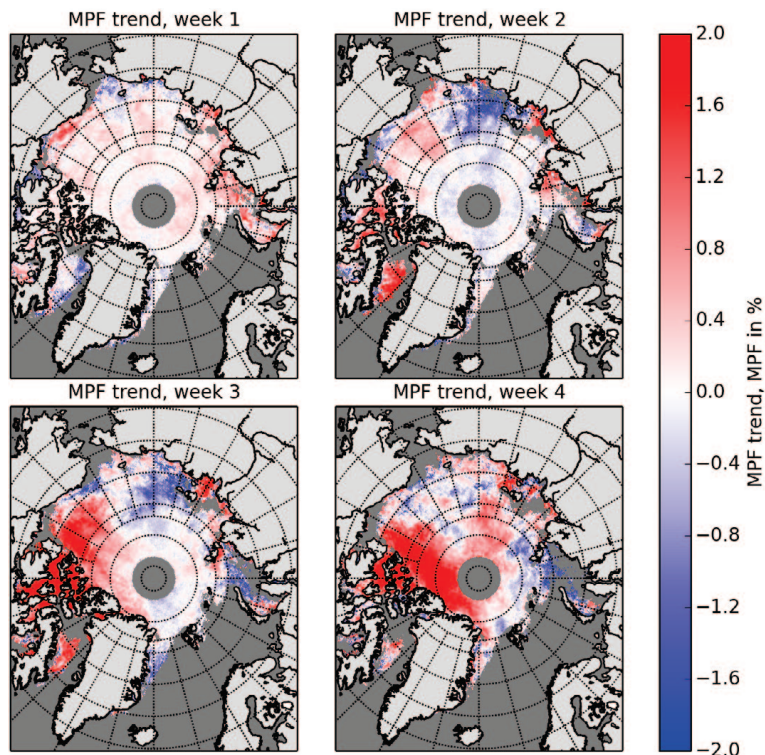


Figure 25. Melt pond fraction trends (trend in MPF %) for the four weeks of June for the whole investigation period 2002–2011.

Title Page

Abstract

Introduction

Conclusions

References

Tables

Figures

◀

▶

◀

▶

Back

Close

Full Screen / Esc

Printer-friendly Version

Interactive Discussion

The melt pond fraction and spectral sea ice albedo retrieval from MERIS data

L. Istomina et al.

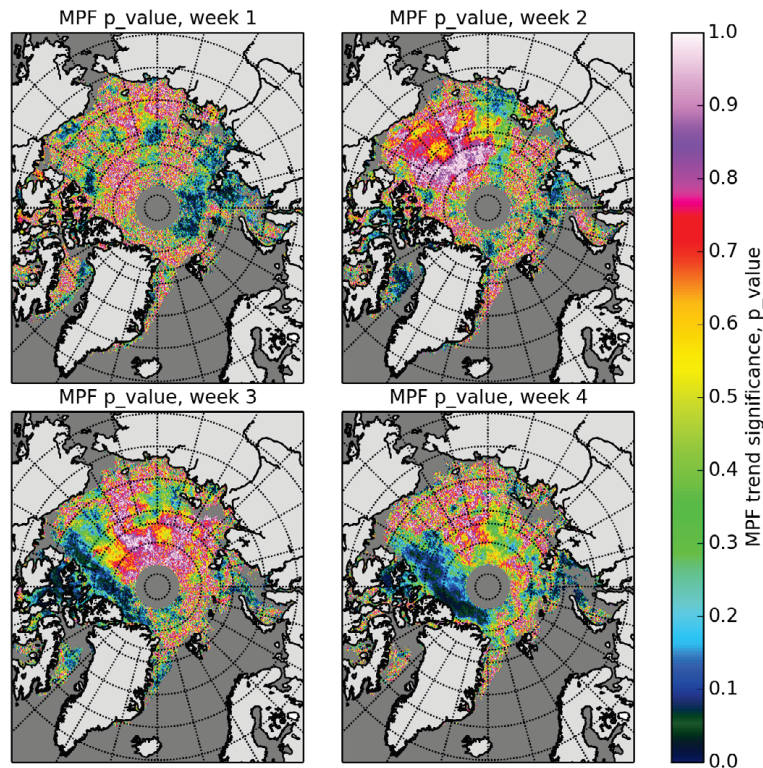


Figure 26. P values for the weekly MPF trends (see Fig. 25).

The melt pond fraction and spectral sea ice albedo retrieval from MERIS data

L. Istomina et al.

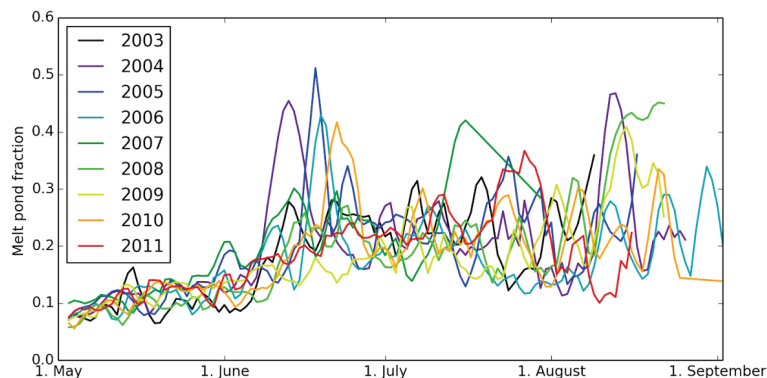


Figure 27. Time sequence of MPF for the studied years for the area of negative MPF trend in the East Siberian Sea. In the 2nd–3rd week of June the MPF in the earlier years of the MERIS dataset reached high (up to 0.5) peak values as the melt onset started, which is typical for the first year ice. In the later years, however, the behavior of the MPF more resembles that on the MYI: no rapid melt onset, lower peak values of MPF. Running mean with window size 3 has been applied to the data.

[Title Page](#)[Abstract](#)[Introduction](#)[Conclusions](#)[References](#)[Tables](#)[Figures](#)[◀](#)[▶](#)[◀](#)[▶](#)[Back](#)[Close](#)[Full Screen / Esc](#)[Printer-friendly Version](#)[Interactive Discussion](#)

The melt pond fraction and spectral sea ice albedo retrieval from MERIS data

L. Istomina et al.

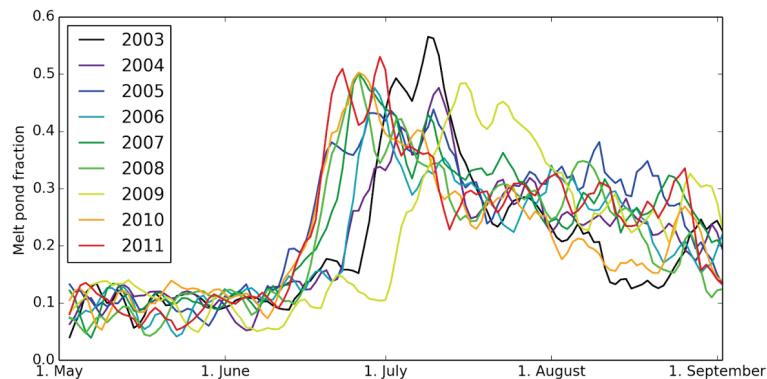


Figure 28. Time sequence of MPF for the studied years for the area of positive MPF trend in the Queen Elizabeth Islands. In the 3rd–4th week of June the MPF in the earlier years of the MERIS dataset reached peak values later in the summer as compared to later years, and melt onset in the later year happens earlier than before. Running mean with window size 3 has been applied to the data.

[Title Page](#)[Abstract](#)[Introduction](#)[Conclusions](#)[References](#)[Tables](#)[Figures](#)[◀](#)[▶](#)[◀](#)[▶](#)[Back](#)[Close](#)[Full Screen / Esc](#)[Printer-friendly Version](#)[Interactive Discussion](#)

The melt pond fraction and spectral sea ice albedo retrieval from MERIS data

L. Istomina et al.

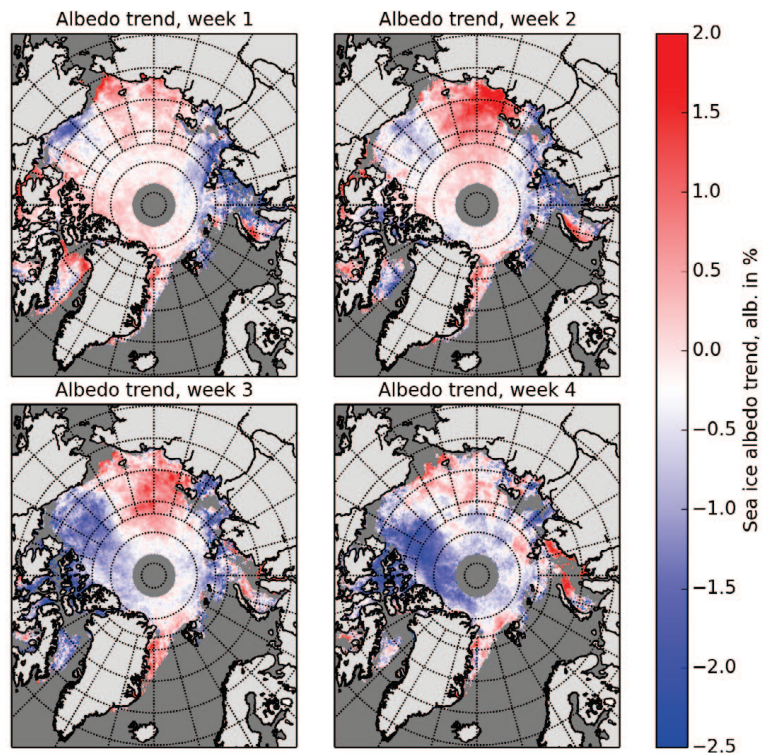


Figure 29. Broadband sea ice albedo trends (trend in albedo %) for the four weeks of June for the whole investigation period 2002–2011.

[Title Page](#)[Abstract](#)[Introduction](#)[Conclusions](#)[References](#)[Tables](#)[Figures](#)[◀](#)[▶](#)[◀](#)[▶](#)[Back](#)[Close](#)[Full Screen / Esc](#)[Printer-friendly Version](#)[Interactive Discussion](#)

The melt pond fraction and spectral sea ice albedo retrieval from MERIS data

L. Istomina et al.

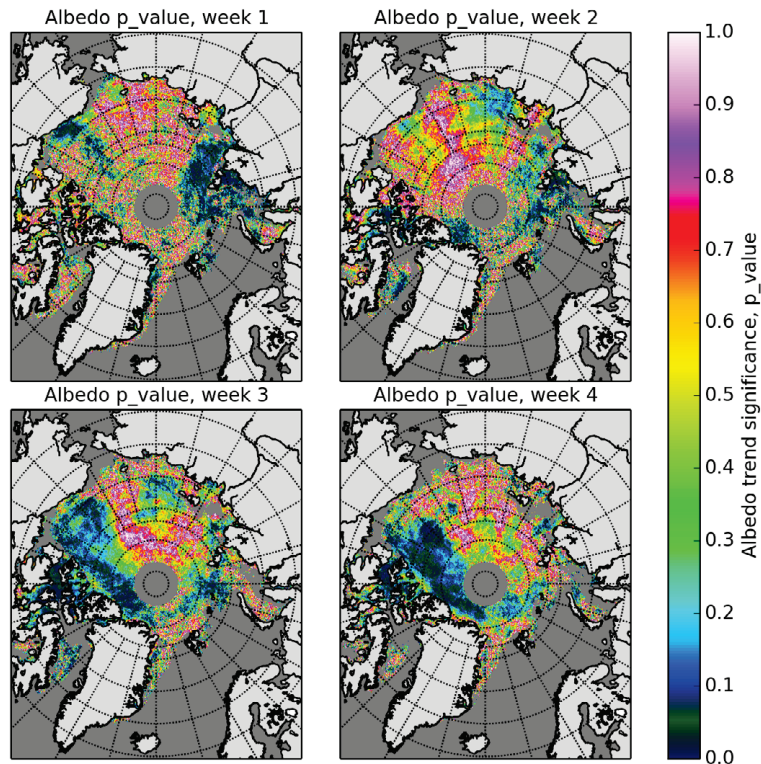


Figure 30. P values for the weekly broadband albedo trends (see Fig. 29).